iScience

CellPress

Article

# Secretagogin Regulates Insulin Signaling by Direct Insulin Binding

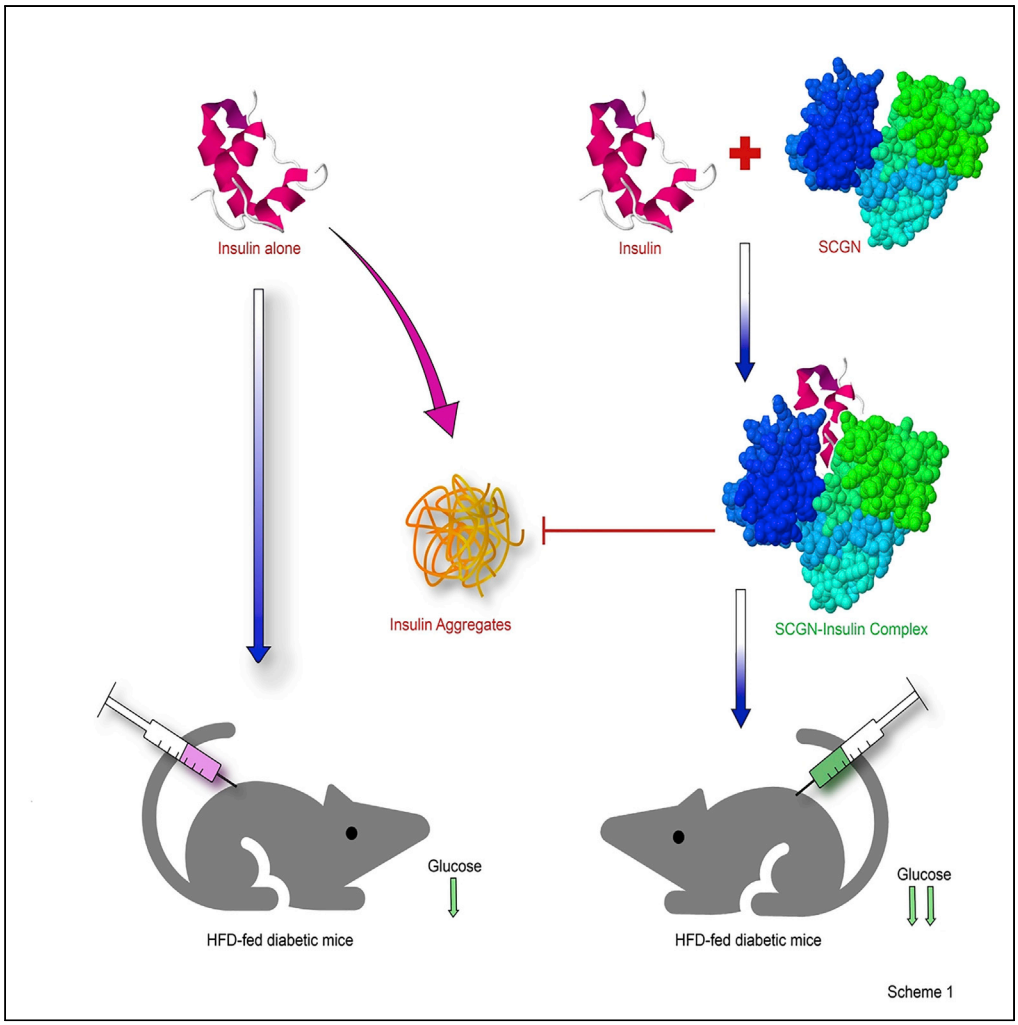


Anand Kumar Sharma, Radhika Khandelwal, M. Jerald Mahesh Kumar, N. Sai Ram, Amrutha H. Chidananda, T. Avinash Raj, Yogendra Sharma

yogendra@ccmb.res.in

## HIGHLIGHTS

SCGN is an insulin-interacting calcium sensor protein

SCGN binding protects insulin from aggregation

SCGN potentiates insulin action *in vivo*

SCGN administration into HFD-fed animals impedes insulin resistance

Sharma et al., iScience *21*, 736–753
November 22, 2019 
https://doi.org/10.1016/j.isci.2019.10.066

iScience

CellPress

Article

# Secretagogin Regulates Insulin Signaling by Direct Insulin Binding

Anand Kumar Sharma,[1,4] Radhika Khandelwal,[1,2,4] M. Jerald Mahesh Kumar,[1] N. Sai Ram,[1] Amrutha H. Chidananda,[1] T. Avinash Raj,[1] and Yogendra Sharma[1,2,3,5,*]

## SUMMARY

**Secretagogin (SCGN) is a β-cell enriched, secretory/cytosolic $Ca^{2+}$-binding protein with unknown secretory regulation and functions. Recent findings suggest that *SCGN* deficiency correlates with compromised insulin response and diabetes. However, the (patho)physiological SCGN-insulin nexus remains unexplored. We here report that SCGN is an insulin-interacting protein. The protein-protein interaction between SCGN and insulin regulates insulin stability and increases insulin potency *in vitro* and *in vivo*. Mutagenesis studies suggest an indispensable role for N-terminal domain of SCGN in modulating insulin stability and function. SCGN supplementation in diabetogenic-diet-fed mice preserves physiological insulin responsiveness while relieving obesity and cardiovascular risk. SCGN-insulin interaction mediated alleviation of hyperinsulinemia by increased insulin internalization, which translates to reduced body fat and hepatic lipid accumulation, emerges as a plausible mechanism for the preservation of insulin responsiveness. These findings establish SCGN as a functional insulin-binding protein (InsBP) with therapeutic potential against diabetes.**

## INTRODUCTION

Peptide-hormone-binding proteins (such as CRH-BPs and insulin-like growth factor-binding proteins [IGFBPs]) bind to the vulnerable peptide hormones, regulating their serum concentration, stability, and activity (Clemmons, 1993; Behan et al., 1995). Insulin is a delicate hormone with aggregation-prone β-chain and redox-sensitive inter/intrachain disulfide bonds (Baker et al., 1988; Hua et al., 1996, 2002). However, in the absence of a bona fide functional insulin-binding protein (InsBP), the understanding of insulin stabilization and activity modulation remains limited. Unlike insulin, IGF (which shares large structural similarities with insulin) signaling employs a dedicated family of IGFBPs) (Clemmons, 1993; Bach, 2015). Thus, as IGFs, insulin intuitively requires a stabilizer/chaperone in the extracellular environment. Several observations prompted us to hypothesize that secretagogin (SCGN) is an InsBP: (1) the existence of SCGN in circulation, (2) abundant expression and partial colocalization with insulin in pancreatic β-cells, and (3) identification of insulin as an interacting partner in our mass-spectroscopy-assisted pull-down of β-cell-specific SCGN-interacting proteins (which we report herein).

Impairment in insulin synthesis, secretion, stability, or sensitivity is responsible for the progression of type 2 diabetes (T2D). Various reports suggest the regulatory role of SCGN in insulin expression and secretion (Wagner et al., 2000; Yang et al., 2016; Kobayashi et al., 2016). Besides, type 2 diabetes patients show reduced SCGN expression (Malenczyk et al., 2017), whereas feeding a diabetogenic high-fat diet (HFD) to mice causes downregulation of SCGN (Hasegawa et al., 2013), implicating SCGN in the pathophysiology of T2D. The reduced SCGN levels in cerebrospinal fluid of insulin-resistant subjects (Westwood et al., 2017) reiterate the involvement of SCGN in insulin resistance. Consistently, the SCGN knockout mice develop glucose intolerance at an early life-stage, which deteriorates progressively to hyperglycemia (Malenczyk et al., 2017), suggesting a confounding role of SCGN in preserving euglycemia. These observations point toward a perplexing correlation between SCGN deficiency and diabetes. Because SCGN deficiency correlates with the incidence of diabetes (Malenczyk et al., 2017; Hasegawa et al., 2013; Westwood et al., 2017), we hypothesized that the exogenous SCGN supplementation would have an anti-diabetic effect *in vivo*.

In this study, using various biophysical and biochemical approaches, we report that SCGN is an insulin-binding protein protecting insulin from physical and chemical stressor-induced aggregation. SCGN also potentiates insulin signaling and hence augments the glucose-lowering activity of insulin *in vivo*. The N-terminal domain of SCGN seems to play an important role in binding and modulating insulin function. The downregulation of SCGN in diabetes led us to investigate if exogenous rSCGN supplementation could

[1]CSIR-Centre for Cellular and Molecular Biology (CCMB), Uppal Road, Hyderabad 500 007, India

[2]Academy of Scientific and Innovative Research (AcSIR), New Delhi, India

[3]Indian Institute of Science Education and Research (IISER), Berhampur, Odisha 760010, India

[4]These authors contributed equally

[5]Lead Contact

*Correspondence: yogendra@ccmb.res.in

https://doi.org/10.1016/j.isci.2019.10.066

rescue from insulin resistance in HFD-fed animals. Our data demonstrate that chronic rSCGN administration preserves the insulin sensitivity in HFD-fed (DIO) animals by promoting insulin clearance, hence alleviating the hyperinsulinemia by the virtue of SCGN-insulin interaction. The insulin-sensitizing effects of rSCGN are detached from the side effects, such as obesity or cholesterol metabolism deregulation. Insulin potentiation and diabetes prevention are the consequences of insulin binding to SCGN. Our data establish SCGN as a functional insulin-binding protein and suggest the translational potential of recombinant SCGN as an anti-diabetic therapy.

## RESULTS

### SCGN Readily Interacts with Insulin: The Synergy of $Ca^{2+}$ and Insulin Binding

In search of novel SCGN interactions and function, we performed a mass-spectroscopy-based pull-down assay from MIN6 cell lysate. We identified several $Ca^{2+}$ binding/chaperone proteins as SCGN interactors. These proteins—binding immunoglobulin protein/78 kDa glucose-regulated protein (BiP/GRP78), protein disulfide isomerase (PDI), 94 kDa glucose-regulated protein (GRP94)—are implicated in the insulin maturation process (Figure 1A). A compelling observation was that, in addition to the aforesaid chaperones, insulin was also captured as an SCGN-interactor. Consolidating previously reported occasional colocalization of SCGN with insulin (Wagner et al., 2000; Gartner et al., 2007), we observed that endogenous SCGN (red) and insulin (green) colocalize (yellow) to a substantial magnitude in insulin-expressing MIN6 cells, which is a pancreatic β-cell line (Figure 1B).

SCGN being a $Ca^{2+}$ sensor (Rogstam et al., 2007), we evaluated the effects of $Ca^{2+}$ on insulin binding using bio-layer interferometry (BLI) analysis (Figure 1C). Recombinant mouse SCGN was prepared as described earlier (Sharma et al., 2015, 2019a, 2019b). We found that apo-SCGN ($Ca^{2+}$-free SCGN) binds insulin with an affinity in the lower micromolar range [$K_d$ = 1.8 μM ($\pm 5 \times 10^{-8}$)], whereas in the presence of $Ca^{2+}$ the overall binding affinity is marginally higher [$K_d$ = 1.4 μM ($\pm 5 \times 10^{-8}$)]. The rate of SCGN-insulin complex formation ($k_{on}$) is of the same order irrespective of the presence of $Ca^{2+}$ [$k_{on}(M^{-1}s^{-1})$ for apo-SCGN= $7.2 \times 10^2$ for holo-SCGN= $4.6 \times 10^2$]. The rate of dissociation in the presence of $Ca^{2+}$ is decreased slightly [$k_{off}(s^{-1})$ for apo-SCGN = $1 \times 10^{-3}$, for holo-SCGN = $6 \times 10^{-4}$], suggesting a strong and specific binding. In the biological context where cytosol has nM [$Ca^{2+}$, whereas the extracellular milieu has mM [$Ca^{2+}$, the apparent lack of $Ca^{2+}$ dependency would make the interaction pervasive. Although more comprehensive titration studies for affinity measurement are required to draw insight, a decreased rate of dissociation in the $Ca^{2+}$-bound form may suggest increased stability of the complex in the $Ca^{2+}$-rich extracellular milieu.

To further validate SCGN-insulin interaction in the extracellular milieu, we performed a protein overlay assay and observed that SCGN binds insulin, irrespective of the presence of $Ca^{2+}$ (Figure 1D). Even partially unfolded insulin (insulin-treated with 4 M urea prior to immobilization) binds to SCGN, suggesting a possibility of SCGN acting as a chaperone for insulin. To examine the physiological occurrence of SCGN-insulin interaction, we performed CoIP experiments from mouse plasma and MIN6 cell lysate/spent media. We found that SCGN, in the animal serum, remains bound to insulin independently of the glycemic status of animals because SCGN was co-precipitated with insulin from the fed/fasting animal serum (Figure 1E). Consistently, in MIN6 cells, we observed a co-precipitation of SCGN with insulin in both the cell lysate and spent media fraction, suggesting an intracellular and extracellular interaction (Figure 1F). Results suggest a universal existence of SCGN-insulin complex in intracellular and extracellular milieu (Figures 1E and 1F). To further affirm if insulin and SCGN form a complex in solution, we performed analytical gel filtration. The holo-SCGN-insulin mixture elutes prior to the holo-SCGN peak (Figure 1G) but not the apo-SCGN (Figure S1), suggesting the formation of a ternary complex between $Ca^{2+}$, SCGN, and insulin. These observations cumulatively establish a pervasive interaction of SCGN with insulin within and beyond pancreatic β-cells.

To gain insight into the effect of $Ca^{2+}$ on SCGN-insulin binding, we performed insulin titration to SCGN solution and examined the change in Trp fluorescence to quantify local changes and monitored tertiary CD fingerprints to analyze global effects. Insulin binding to holo-SCGN leads to a more prominent reduction in the fluorescence intensity than to apo-SCGN (Figures S2A and S2B), suggesting a positive modulation by $Ca^{2+}$. Because the blue-shifted spectrum is a hallmark of $Ca^{2+}$-bound SCGN (Rogstam et al., 2007), the apparent absence of insulin-induced shift in λmax in holo-SCGN suggests that $Ca^{2+}$ is neither replaced nor removed allosterically by insulin. The mutual independence of $Ca^{2+}$ and insulin binding to SCGN is further supported by near-UV circular dichroism spectral analysis. Insulin binding induces conformational

A

| Accession no. | Protein name | Unique peptides | Function |
|---|---|---|---|
| IPI00319992.1 | 78 kDa Glucose-Regulated Protein (BiP) | 2 | Molecular chaperone of endoplasmic reticulum (ER) |
| IPI00854971.1 | Protein Disulfide-Isomerase A6-like | 2 | Chaperone, $Ca^{2+}$ binding |
| IPI00133522.2 | Protein Disulfide-Isomerase | 1 | Chaperone, $Ca^{2+}$ binding |
| IPI00230108.6 | Protein Disulfide-Isomerase A3 | 5 | Chaperone, $Ca^{2+}$ binding |
| IPI00129526.1 | Endoplasmin (GRP-94) | 2 | Chaperone, $Ca^{2+}$ binding, UPR response |
| IPI00134310.3 | Insulin (Ins1)* | 1 | Peptide hormone |
| IPI00134311.1 | Insulin (Ins2)* | 3 | Peptide hormone |

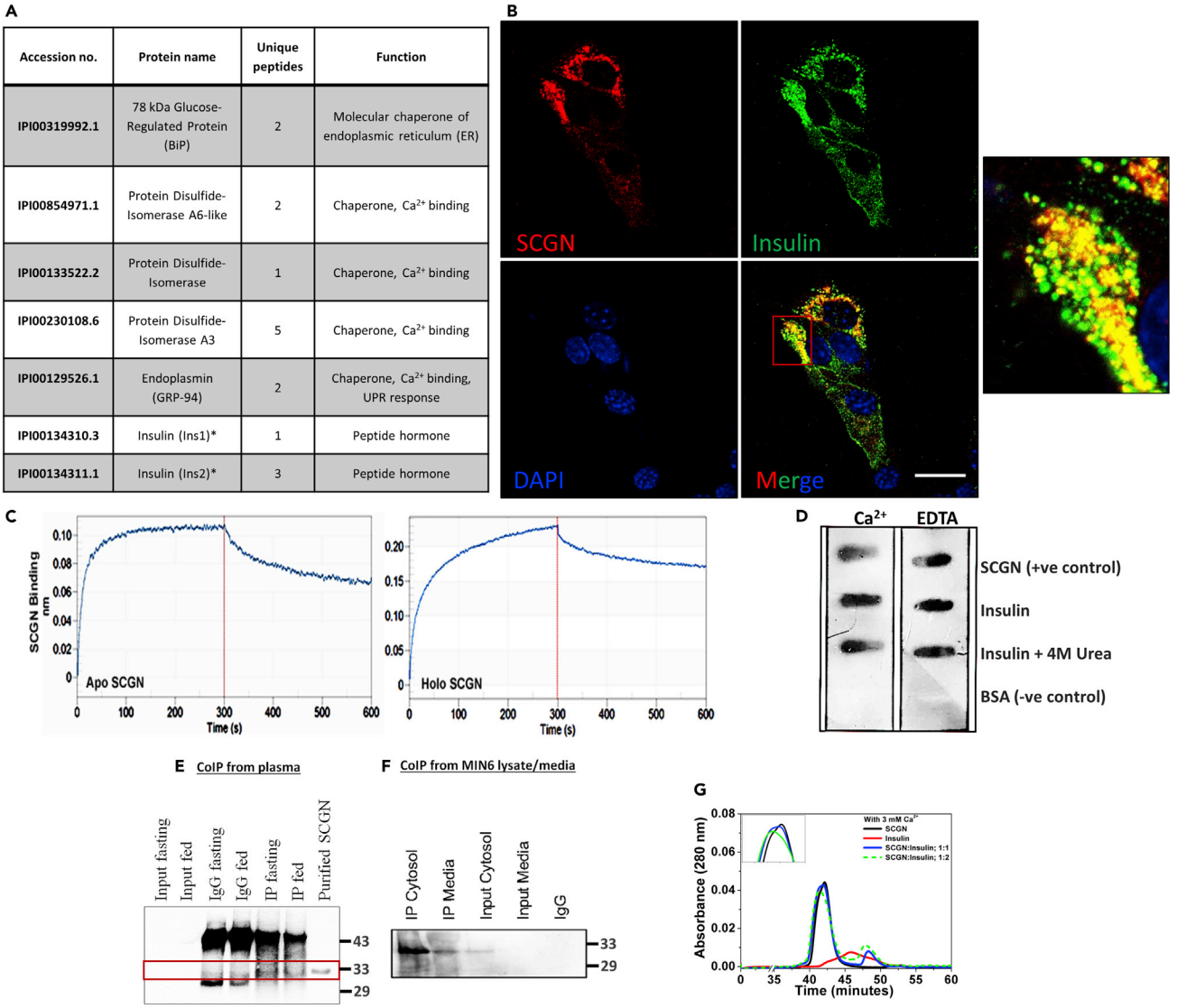


**Figure 1. SCGN Interacts with Insulin *in vitro* and *ex vivo***

(A) List of SCGN interacting partners identified in mass-spectrometry-assisted pull-down assay.

(B) Microscopy images depicting colocalization (yellow) of SCGN (red) and insulin (green) immunostained with Alexa Fluor 594 (red) and Alexa Fluor 488 (green) respectively in MIN6 cells. Scale bar, 20 μm.

(C) BioLayer interferometry (BLI) binding curve of SCGN-insulin interaction. The data were fit in 1:1 model [$R^2$ for apo-SCGN-insulin experiment is 0.9547 ($Chi^0$ value is 0.004) and for holo-SCGN-insulin binding is 0.9626 ($Chi^2$ value being 0.0126)].

(D) Protein overlay assay to assess the SCGN-insulin interaction.

(E and F) CoIP from animal plasma and MIN6 cell lysate showing *in vivo* interaction of SCGN with insulin in both cellular and extra-cellular milieu.

(G) Analytical size-exclusion chromatography of SCGN, insulin, and SCGN-insulin mixture in 1:1 and 1:2 stoichiometric ratios in the presence of $Ca^{2+}$ representing a distinct complex formation between SCGN and insulin.

changes similar to $Ca^{2+}$. Insulin also induces similar changes in near-UV CD spectrum of $Ca^{2+}$-SCGN producing similar conformational changes irrespective of the order of the ligand (Figures S2C and S2D). These results establish SCGN as an insulin-binding protein with scope for positive modulation by $Ca^{2+}$.

## SCGN Protects Insulin from Aggregation and Fibrillation and Alleviates Fibril Toxicity

The major regulation of insulin action is supposed to be achieved at the insulin secretion level. Structural stabilization and activity modulation of circulatory insulin, however, remain poorly understood. Because insulin has a soaring propensity to form cytotoxic fibrils and because SCGN was found to interact even with

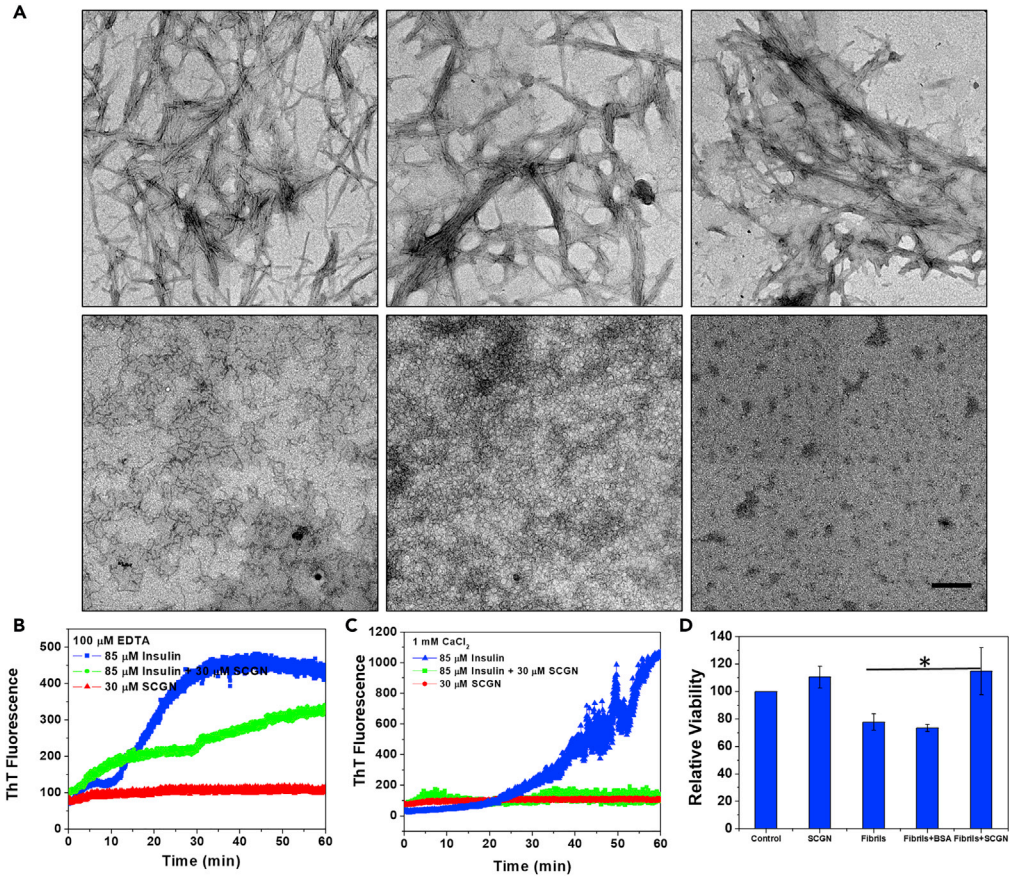


**Figure 2. SCGN Protects Insulin from Aggregation and Fibrillation and Reduces Cytotoxicity *ex-vivo***

(A) Transmission electron microscope (TEM) images depicting the inhibition of insulin fibrillation by SCGN.

(B and C) Time scan spectra representing the change in the emission of ThT fluorescence of insulin fibrillation in the presence of SCGN (1:2 ratio) in its apo- or holo-form. Scale bar, 0.6 μm.

(D) MTT cell viability assay demonstrating the role of SCGN in alleviating cell cytotoxicity caused due to insulin fibrils in MIN6 cells.

Error bars represent mean ± SEM (fibrils vs (fibril + SCGN) *p value = 0.034).

denatured insulin suggestive of chaperone property (Figure 1D), we speculated that SCGN would protect insulin from detrimental misfolding and aggregation. Consistently, we observed that SCGN impedes heat-induced fibrillation of insulin (Figure 2). The inhibition of the nucleation of fibrillation is largely independent of $Ca^{2+}$ because the apo- as well as holo-SCGN inhibit insulin fibrillation (Figure 2A; vertical panels 1 and 2). Unexpectedly, SCGN could also dissolve preformed fibrils within an hour under the given experimental conditions (Figure 2A; last panel). Measurements of the rate of fibril formation using the fluorescent probe thioflavin T (ThT) show that apo-SCGN exerts ~50% protection against heat-induced amyloidogenesis of insulin (Figure 2B), whereas holo-SCGN completely abolishes the fibrillation of insulin (Figure 2C).

The protection exerted by SCGN is also visible in the disulfide-bond reduction-induced aggregation of insulin. Apo-SCGN rescues insulin from aggregation in a dose-dependent manner (Figure S3), implying that apo-SCGN stabilizes insulin, likely by providing a niche to protect the exposed disulfide bonds involved in interchain disulfide bridge formation. These results demonstrate that SCGN prevents insulin misfolding and aggregation and shears existing fibrils. Because of their cytotoxicity, fibrils have been implicated in various neurodegenerative diseases and in diabetes (Schneider et al., 1980; Maloy et al., 1981; Höppener et al., 2000; Ross and Poirier, 2004; Muchowski and Wacker, 2005; Wang et al., 2010). We verified if SCGN alleviates cytotoxicity caused by insulin fibrils *ex vivo*. Consistently, exogenous SCGN reduces insulin fibril toxicity significantly in MIN6 cells (Figure 2D). BSA, which was included as a control, did not exert any protection. These results suggest that SCGN effectively inhibits the fibrillation of insulin, dissolves the

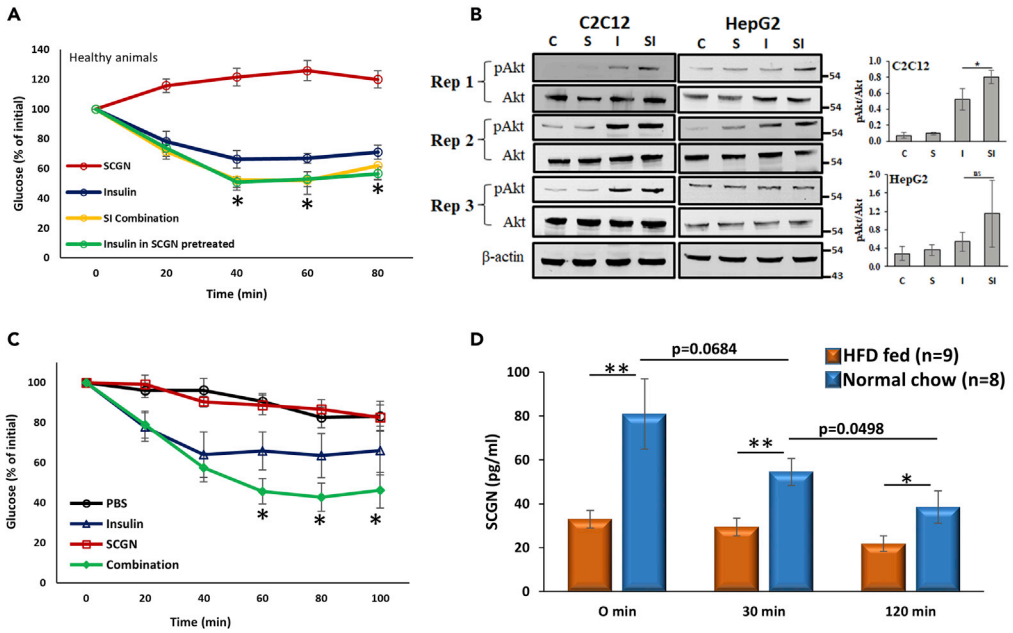


**Figure 3. SCGN Potentiates Insulin Signaling**

(A) ITT of BALB/c mice injected with either insulin, SCGN, or combination of insulin and SCGN after 6-h fasting.

(B) Western blots and corresponding densitometry analysis showing the increased insulin-induced phosphorylation of Akt in the presence of SCGN in differentiated C2C12 and HepG2 cells.

(C) ITT in STZ animals after injection of SCGN or insulin or a combination.

(D) Serum SCGN concentration of C57BL/6 mice maintained on normal chow-diet (blue bars) or HFD (pink bars) as measured by ELISA at different time points in OGTT paradigm.

Error bars represent mean ± SEM. *= p<0.05, **= p<0.01.

preformed fibrils, and alleviates the fibril-associated cytotoxicity. The chaperone interactome (Figure 1A) and the observed anti-amyloid properties of SCGN suggest that SCGN is a molecular chaperone.

## SCGN Improves Insulin Signaling

Having established the SCGN-insulin interaction, we next studied the effect of SCGN on physiological insulin signaling. We hypothesized that if the described results were a consequence of a biologically relevant and functional SCGN-insulin interaction, SCGN would increase insulin potency *in vivo*. To test the hypothesis, we performed an insulin tolerance test (ITT) in healthy mice (Figure 3A). Each group of animals received one of the following treatments: (1) recombinant SCGN (rSCGN), (2) insulin, (3) SCGN-insulin combination, or (4) insulin into the rSCGN-pretreated animals. rSCGN injections were inconsequential, whereas administration of SCGN-insulin combination was more effective in clearing blood glucose than insulin (Figure 3A). Owing to the apparent lack of glucose clearance by SCGN alone, the enhanced potency of SCGN-insulin combination is attributed to SCGN-insulin interaction. To validate the data, we analyzed the ability of insulin or insulin-SCGN combination to induce Akt phosphorylation in two relevant cell lines (HepG2 and C2C12 myotubes). We found statistically increased Akt phosphorylation in C2C12 myotubes treated with SCGN-insulin combination when compared with cells treated with insulin alone (Figure 3B). However, in the case of HepG2, the effect is insignificant, which may suggest a need for additional cofactors or a tissue-specific modulation of insulin action by SCGN. These results demonstrate that SCGN enhances insulin signaling consistent with *in vivo* data.

Secretagogin-induced lowering of glucose in mice compelled us to explore if SCGN wields insulin mimic activity *in vivo*. To check this, we injected SCGN to β-cell-deficient streptozotocin (STZ)-treated mice. rSCGN injection does not elicit any glucose-lowering effect, thus ruling out the possibility of insulin-mimetic activity of SCGN (Figure 3C). Even in STZ animals, substantiating the physiological importance of SCGN-insulin interaction, the SCGN-insulin combination was found to be more potent than insulin. These findings established that SCGN could increase the potency of exogenous insulin. Our data may offer an explanation to the cause of compromised insulin response in the SCGN knockout upon glucose

challenge (Malenczyk et al., 2017). These results suggest that SCGN is a physiological modulator of insulin signaling. Consistently, SCGN was always present in the serum of healthy animals (Figure 3D). In the oral glucose tolerance test (OGTT) paradigm, fasting SCGN concentration was found to be higher. An oral glucose gavage led to a reduction in SCGN concentration, which significantly drops after 120 min (Figure 3D). However, consistent with the reported downregulation of SCGN in diabetic subjects (Malenczyk et al., 2017), we noted a significant reduction in serum SCGN concentration of HFD-fed mice at all time-points in OGTT paradigm (Figure 3D). This may suggest that at hypoglycemic levels, SCGN concentration remains high. Once circulatory glucose levels increase, abundant SCGN binds insulin to help it function appropriately. As the insulin levels subside after 120 min of glucose administration, SCGN levels also drop correspondingly. This suggests that there is an intricate coherence in SCGN secretion, which is disturbed in pathophysiology.

### SCGN N-terminal Domain Is Essential for Functional Modulation of Insulin

We then directed our efforts to map the individual domains responsible for insulin binding and the biological properties. We first modeled the SCGN-insulin complex using Patchdoc software (Schneidman-Duhovny et al., 2005). The initial analysis suggests that all the three lobes of SCGN participate in insulin binding, thus complicating the experimental analysis of the precise binding site (Figure 4A). Based on this information, two truncated versions of SCGN lacking either N-terminal (ΔNTD) or C-Terminal (ΔCTD) domain were designed (Figure 4B). The insulin binding examined by protein overlay assay suggested a preserved (but weaker) insulin binding to both the truncations (Figure 4C), which is anticipated from the large contact area in SCGN-insulin complex. Similarly, *in vitro* insulin potentiation was unaffected by deletions (Figure S4), suggesting that middle domain of SCGN may have a primary role in establishing insulin contact and modulating insulin functions. Nonetheless, in Trp fluorescence, we observed that addition of insulin brought more prominent changes in ΔCTD than ΔNTD, suggesting a stronger binding to ΔCTD (Figure S5). Similarly, when we monitored anti-fibrillar activity of truncated proteins for insulin by TEM, ΔNTD showed compromised protection of insulin from aggregation while ΔCTD is unaffected (Figures2A and 4D). This suggests that N-terminal domain of SCGN is important for a tight insulin binding and thereby for inhibition of fibrillation. Consistently, ThT fluorescence also demonstrated compromised protection of insulin by ΔNTD (both the apo- and holo-forms), whereas ΔCTD showed enhanced protection in the presence of $Ca^{2+}$, which was comparable to full-length SCGN (Figures 4E and 4F). We performed these studies at three different SCGN concentrations to examine dose-response and found that 20 μM ΔCTD (as full-length SCGN) showed complete protection while ΔNTD was relatively ineffective (Figure S6). Although at high concentrations BSA also inhibits insulin fibrillation (Finn et al., 2012) (Figures 4E and S7), the effect of SCGN was much more prominent even at lower concentration (1:10 protein:insulin stoichiometry), suggesting a specificity of insulin chaperoning by SCGN. Moreover, TEM imaging suggested that the inhibition by BSA was partial as visible insulin fibrils were present in the presence of BSA (Figure S7). The ThT fluorescence or the fibrils visualized by TEM were not due to protein, as alone protein did not exhibit any ThT fluorescence or visible fibrils on TEM (Figures S6 and S8).

We then sought to check if *in vivo* effects of SCGN on insulin potentiation are preserved in truncated proteins. Intriguingly (and consistent with anti-fibrillation results), ΔCTD was as effective as full-length SCGN in potentiating insulin signaling when co-administered with insulin (Figure 4G). In contrary, the deletion of the N-terminal domain completely obliterates SCGN's ability to potentiate insulin (Figure 4G). These effects were insulin-dependent, as no reduction in blood glucose was seen in animals injected with only SCGN protein (Figure 4H). The maintenance of *in vitro* insulin modulatory activity of ΔNTD is likely due to the slack binding of insulin and simplicity of the system. Contrary to inclined cellular system, when ΔNTD is co-administered with insulin *in vivo*, the changing microenvironment and absorption process leads to dissociation of the weak ΔNTD-insulin complex, thus the interaction becomes inconsequential. These results demonstrate specificity of insulin binding to SCGN with an imperative role for the N-terminal domain of SCGN for efficacious insulin binding while C-terminal domain is dispensable.

### Chronic SCGN Administration Preserves Insulin and Glucose Tolerance and Lowers Hyperglycemia in an Insulin-Dependent Manner

Insulin resistance is a physiological state where insulin, despite its (abundant) presence, cannot induce the clearance of circulating glucose. To ascertain if the exogenous rSCGN administration could rescue HFD-fed animals from systemic insulin under-responsiveness and to explore the therapeutic potential of these findings in diabetes, we systematically studied the effect of rSCGN administration in insulin-resistant

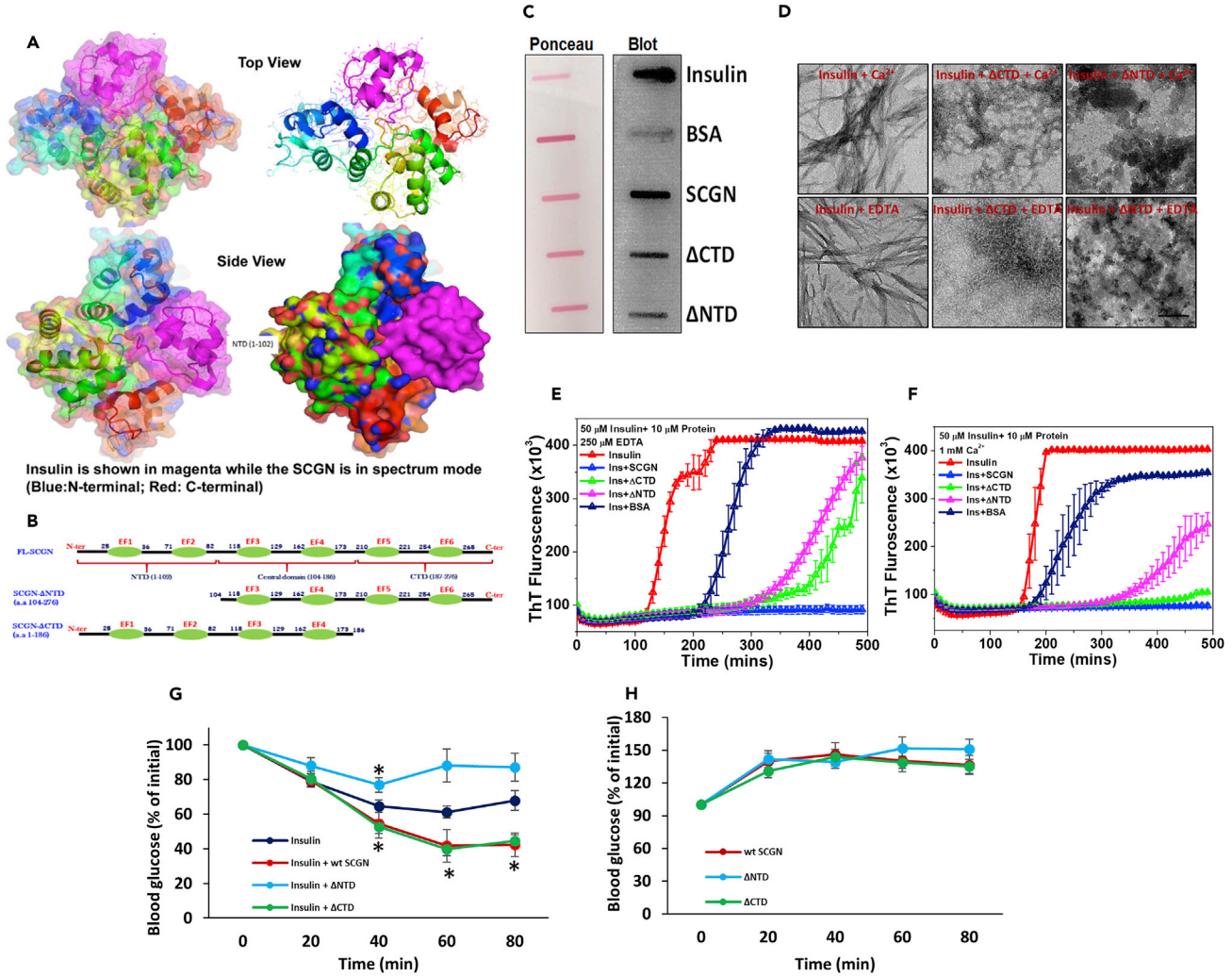


**Figure 4. SCGN N-terminal Domain Imparts Specificity and Functionality**

(A) SCGN-insulin-complex model showing a large surface contact area between SCGN and insulin.

(B) Truncation strategy to generate N-terminal or C-terminal deleted SCGN.

(C) Protein-overlay assay suggesting a preservation of insulin binding to domain deleted mutants of SCGN.

(D) TEM images depicting a compromised chaperoning of insulin by ΔNTD but the upholding of the same in ΔCTD. Scale bar, 0.2 μm.

(E and F) ThT fluorescence (intermittent readings) representing a compromised protection by ΔNTD but a better protection by ΔCTD under given conditions. *Please note that same insulin aggregation profile is used in both panels (and associated supplementary information) as the data are derived from the same experiment.*

(G) ITT with truncated SCGN showing a loss of insulin potentiation by ΔNTD, whereas the ΔCTD is as effective as full-length SCGN, (H) blood glucose levels after administration of truncated SCGN showing no reduction in glucose level. Error bars represent mean ± SEM. *= $p<0.05$.

animals. Because the diet-induced obese (DIO) animal model mimics the multifactorial human lifestyle-associated diabetes better than monogenic knockout animal models, we utilized DIO mice to examine the insulin-sensitizing activity of exogenous SCGN. We designed an *ab initio* SCGN-treatment protocol, wherein the treatment group received a subcutaneous rSCGN injection every other day from day 1 of exposure to the confounding factor (i.e., HFD), whereas control groups (HFD and normal-chow fed) received phosphate buffered saline (PBS) injections. After 12 weeks of exposure to HFD and concurrent treatment, the effect of rSCGN administration on insulin and glucose tolerance was assessed (Figures 5A and 5B upper and lower panels). Upon exogenous insulin injection, rSCGN-treated HFD-fed animals cleared blood glucose more efficiently than control HFD despite the adversity of higher initial blood glucose level (t = 0 in ITT) (Figure5A). However, the statistically significant glucose lowering was achieved only after 60 min of insulin injection. Therefore, SCGN-mediated increase in glucose clearance might not reflect a

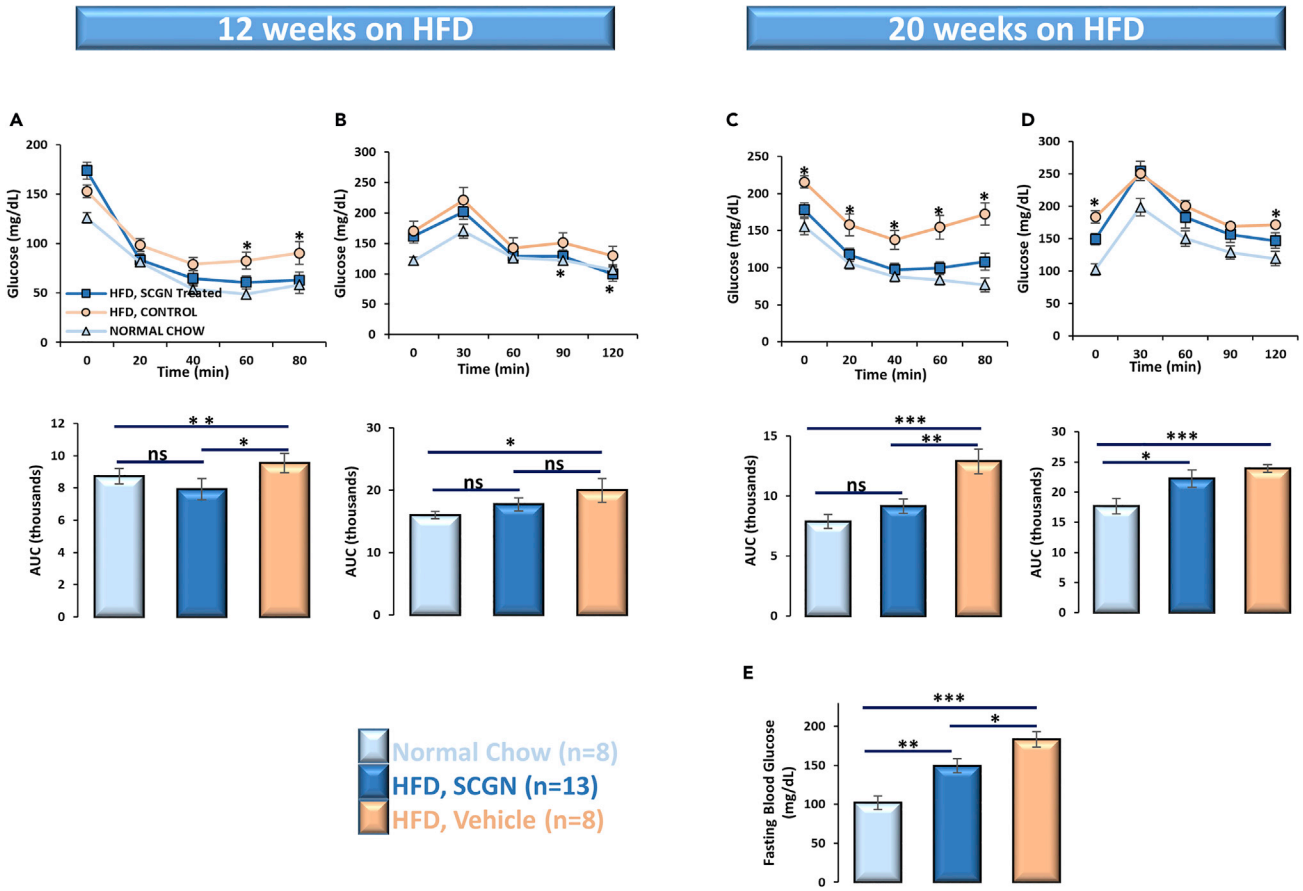


**Figure 5. Chronic SCGN Administration Lessens Insulin Resistance in DIO Animals**

(A) ITT of chow-/HFD-fed animals after 12 weeks of exposure to HFD.

(B) OGTT of the animals after 12 weeks. ITT and OGTT were repeated after an additional two months of SCGN treatment (or vehicle injection).

(C–E) (C) ITT; (D) OGTT; (E) fasting blood glucose levels of DIO mice (0-min glucose values in last OGTT).

Error bars represent mean ± SEM. *= p<0.05, **= p<0.01, ***= p<0.001.

direct effect on insulin action, and additional work is required to understand the potential impact of SCGN on insulin sensitivity. To check if the same is true for endogenous insulin, we performed an oral glucose tolerance test (OGTT). Although the initial blood glucose levels of both treated and untreated HFD-fed animals were high, rSCGN-treated animals efficiently cleared excess glucose from the blood and achieved a normoglycemia comparable to the normal-diet-fed animals (Figure 5B).

Encouraged by these results, we continued HFD and concomitant rSCGN administration for an additional two months to assess the efficacy of treatment on the severity of insulin resistance and hyperglycemia. At the conclusion of the experimental period, we found that rSCGN-treated HFD-fed animals had complete preservation of insulin sensitivity, comparable to the chow-fed control animals (Figure 5C). Glucose was better cleared in rSCGN-treated HFD-fed animals when compared with the untreated HFD group (Figure 5D). These results are better reflected in fasting blood glucose (derived from t = 0 of OGTT) levels, where the rSCGN-treated animals have lower blood glucose levels reflecting better glycemic control and sustenance of normoglycemia (Figure5E). These results suggest that SCGN supplementation improves insulin response and point toward the anti-diabetic potential of SCGN.

## SCGN-mediated Alleviation of Hyperinsulinemia Prevents Insulin Resistance

Pronounced preservation of insulin sensitivity in rSCGN-treated HFD-fed mice intrigued us to explore the mechanism of persistent insulin responsiveness. We found that the control chow group had expected normal insulin concentration. However, untreated HFD-fed animals had much higher circulating insulin

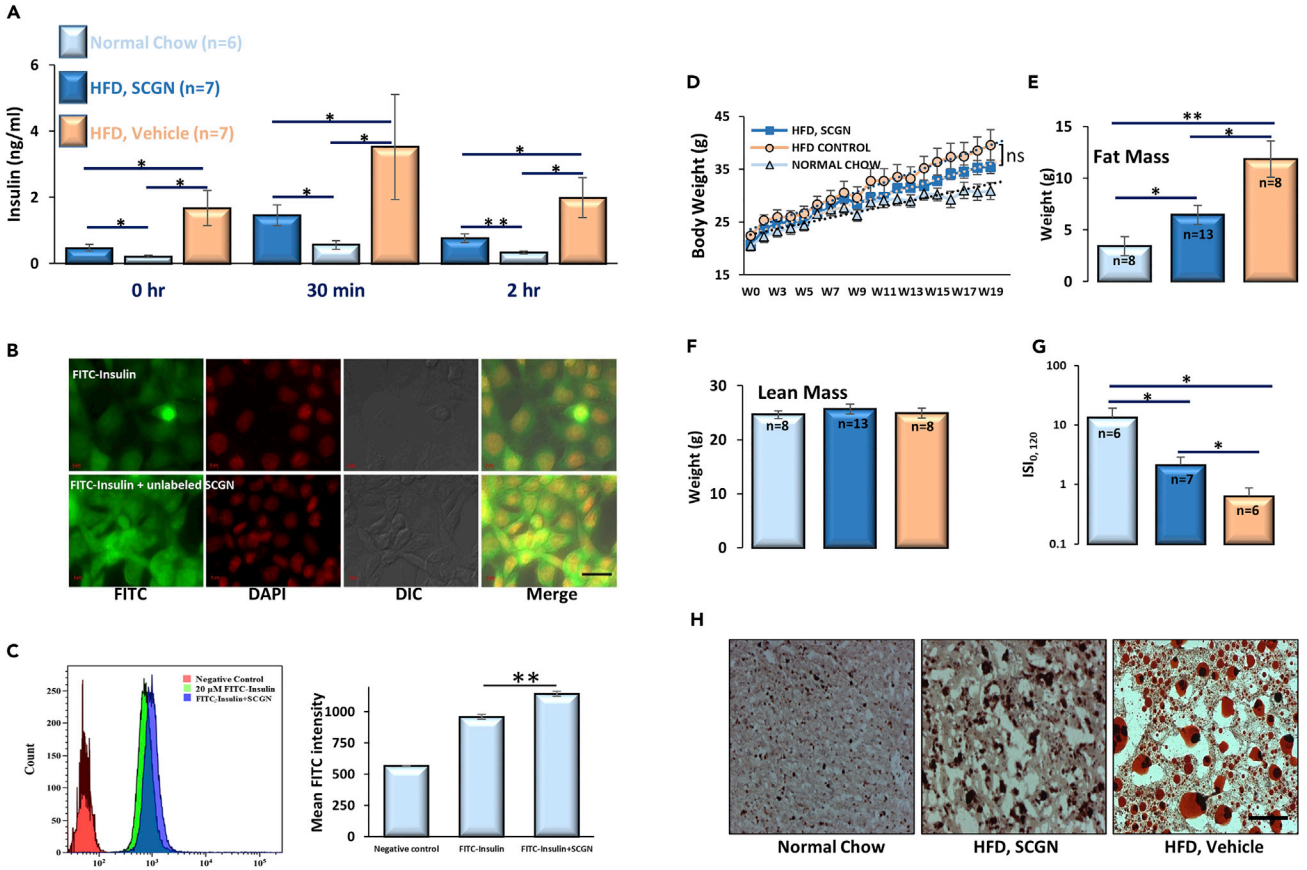


**Figure 6. SCGN Administration Moderates Hyperinsulinemia and Body/Liver Fat Deposition**

(A) Serum insulin concentration measured by ELISA in the same cohort of animals at different time points in OGTT paradigm.

(B) Microscopic images showing increased internalization of FITC-insulin conjugate into HepG2 cells in the presence of unlabeled SCGN. FITC-labeled insulin (10 μM) and 10-μM FITC-insulin mixed with unlabeled SCGN were incubated for an hour followed by acid buffer wash, fixation by formaldehyde, and subsequently mounted on slides, Scale bar (right bottom), 20 μm.

(C) FACS-mediated quantification of FITC-insulin conjugate internalization in the presence and absence of SCGN.

(D) Change in body weight in the same cohort of animals over a period of 20 weeks.

(E) Total body fat measured by echoMRI.

(F) Lean mass (differences between the groups are insignificant).

(G) Insulin sensitivity index ($ISI_{0,\ 120}$).

(H) Oil Red O staining of liver cryosections. Scale bar, 100 μm.

Error bars represent mean ± SEM. *= p<0.05, **= p<0.01.

level at different time points in the OGTT paradigm, whereas rSCGN-injected animals showed reduced insulin levels (Figure 6A). Because sustained hyperinsulinemia is an established determinant of insulin resistance (Czech, 2017), and because SCGN is already shown to positively regulate the expression and secretion of insulin (Wagner et al., 2000; Malenczyk et al., 2017), we were perplexed with the reduction of insulin levels on SCGN administration. We thus examined if SCGN binding could induce the clearance of circulatory insulin post-secretion. For this purpose, we designed an *in vitro* insulin clearance assay wherein fluorescently labeled insulin was incubated with physiologically relevant hepatic cell line, HepG2. Consistent with our post-secretion clearance hypothesis, SCGN increases the FITC-insulin clearance to a visually appreciable extent seen as cell-internalized fluorescence (Figure 6B). In addition, in the presence of SCGN, there were more visible puncta or granular structures, pointing toward improved vesicular endocytosis (of the insulin-IR complex) by SCGN. We validated microscopy data with FACS-assisted quantification of FITC-insulin internalization (Figure 6C). The intensity of the internalized FITC-insulin was higher in the presence of SCGN than in the absence thereof. The increased insulin internalization was also seen in ELISA mediated insulin clearance using hepatic cell line but not in non-hepatic N2A neuroblastoma cells (Figures S9A and S9B). Nonetheless, it is the anatomic design that liver is the first organ

exposed to secreted insulin. Thus, even though other organs/cells may be capable of insulin degradation, they do not encounter high insulin concentration in healthy conditions. These results suggest that SCGN facilitates the hepatic clearance of circulatory insulin, thus retarding the progression of insulin resistance.

Hyperinsulinemia underwrites the weight gain (Pories and Dohm, 2012; Corkey, 2012; Vernochet et al., 2012; Pedersen et al., 2015; Templeman et al., 2015; D'souza et al., 2016), and resulting obesity is a major risk factor for lifestyle-associated diabetes and insulin resistance (Samuel and Shulman, 2012). Thus, we monitored weight gain in animals by HFD. rSCGN-treated animals had an insignificant reduction in weight gain than untreated HFD-fed animals (Figure 6D). Nonetheless, the rSCGN-treated animals had significantly lower body fat than untreated HFD-fed mice while the lean mass was comparable (Figures 6E and 6F). These results suggest that SCGN-mediated insulin clearance alleviates hyperinsulinemia in HFD-fed animals, which transcribes into the reduced body fat. To test if SCGN induced preservation of metabolic features specific to the diabetogenic diet-fed state, we performed a short control study on another cohort of mice fed either a normal chow or HFD (Figure S10). The SCGN administration to normal chow-fed animals was largely inconsequential (Figure S10). After six weeks of SCGN treatment, the ITT, OGTT, and weight gain were same in treated vs untreated normal chow-fed animals (Figures S10A–S10C), whereas the HFD-fed mice treated with SCGN showed a better insulin tolerance than untreated HFD mice (Figure S10D). This suggests that SCGN administration does not cause a negative effect in healthy animals but imparts beneficial effects under diabetogenic conditions.

To calculate the extent of insulin sensitivity in control HFD group and to find the extent of protection exerted by SCGN administration, we calculated the insulin sensitivity index, $ISI_{(0,\ 120)}$ (Gutt et al., 2000). The normal chow-fed animals had the best insulin sensitivity; rSCGN-treated mice had significantly higher $ISI_{(0,\ 120)}$, suggesting a better insulin sensitivity than in untreated HFD-fed animals (Figure 6G). However, further work needs to be done to understand whether SCGN potentiates/preserves/improves insulin action/sensitivity directly by modulating insulin signaling in probably a tissue-specific manner (as demonstrated in Figure 3) or indirectly through its effects on parameters such as body weight and fat mass composition (Figure 6).

In addition to reduced body fat, Oil red O staining demonstrated reduced hepatic triglycerides and lipid levels in rSCGN-treated HFD animals when compared with that of the HFD control group (Figure 6H). SCGN-treated HFD-fed animals exhibited significantly reduced Oil red O staining, demonstrating reduced hepatic triglyceride/lipid accumulation (Figure S9C). Hepatic steatosis symptoms were alleviated in SCGN-treated animals, with smaller lipid droplets and reduced necrotic areas (Figure 6H). Growing results suggest that hepatic lipid accumulation profoundly contributes to insulin resistance (Perry et al., 2014). Thus, SCGN administration induces the lowering of hepatic lipid deposition, which also contributes to the sustenance of insulin sensitivity.

### Systemic Protection in DIO Mice after SCGN Administration

Altered body fat composition leads to adjusted lipid metabolism, which precipitates the risk of cardiovascular diseases (Van Gaal et al., 2006). We tested the effect of rSCGN treatment on serum lipid profile and other related factors (Figures 7A–7E). rSCGN administration marginally reduced total serum triglyceride level, whereas cholesterol levels were significantly reduced when compared with untreated HFD-fed animals (Figures 7A and 7B). The reduction in total cholesterol is likely due to a reduction in low-density lipoprotein (LDL) concentration because high-density lipoprotein level remains comparable to untreated animals (Figures 7C and 7D), suggesting that rSCGN treatment mitigates the obesity-associated risk of cardiovascular diseases. Because SCGN is a redox-responsive $Ca^{2+}$ sensor (Rogstam et al., 2007; Khandelwal et al., 2017) and altered serum $Ca^{2+}$ concentration is a marker for early stage insulin resistance (Thalassinos et al., 1993; Becerra-Tomás et al., 2014; Rooney et al., 2016; Holmes, 2016), we also measured the serum $Ca^{2+}$ concentration. This is also important to validate that rSCGN administration does not quench the plasma $Ca^{2+}$ that may affect the systemic physiology negatively. The untreated HFD-fed mice had morbidly higher serum $Ca^{2+}$ levels, whereas rSCGN-treated animals had normalized levels comparable to normal chow-fed group, reconfirming preserved insulin sensitivity in rSCGN-treated HFD-fed animals (Figure 7E).

We next compared the histology of selected tissues of the animals. Because SCGN is highly expressed in pancreatic β-cells, we examined pancreatic histology to rule out negative effects of exogenous rSCGN (e.g., by immune activation, that will be reflected in islet loss) on islet integrity. rSCGN-treated animals

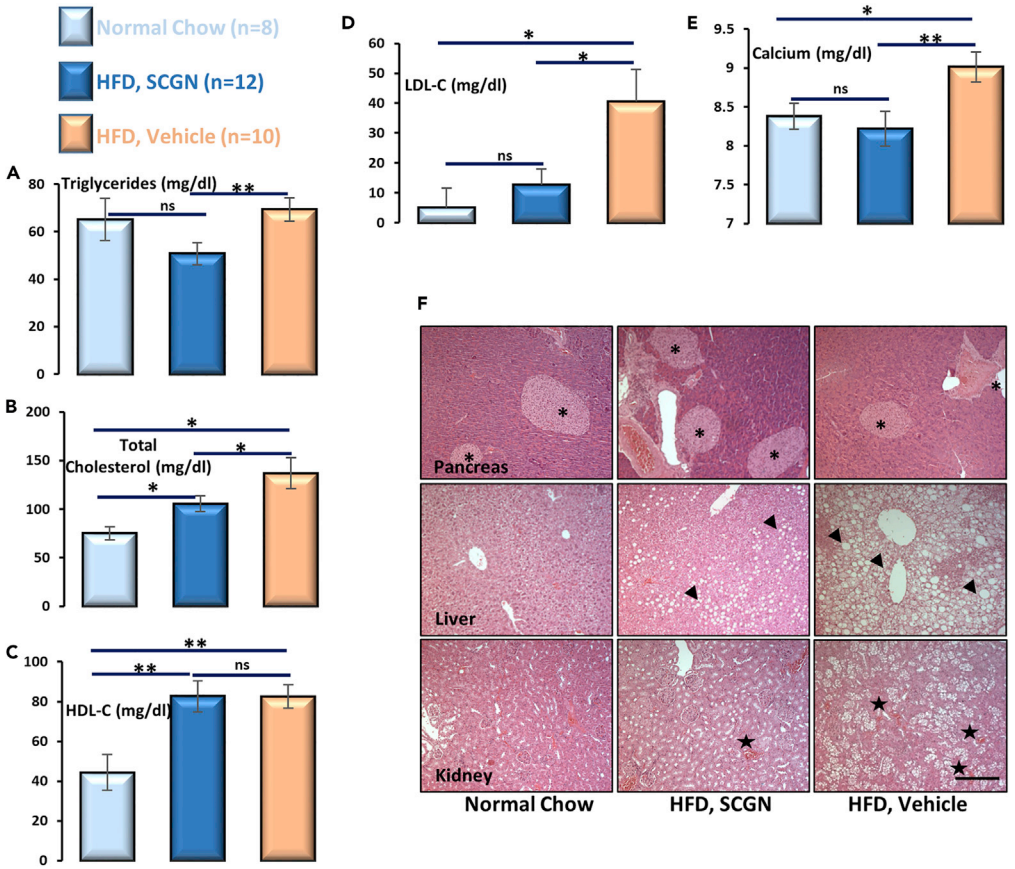


**Figure 7. SCGN Administration Elicits Systemic Protection**

Serum and tissues were collected at the end of study.

Serum analysis of (A) total triglyceride; (B) cholesterol; (C) HDL cholesterol; and (D) LDL cholesterol; (E) $Ca^{2+}$; estimation was performed as as per kit guidelines.

(F) H&E staining of pancreas, liver, and kidney sections was performed with formalin fixed tissue following standard protocol. Scale bar, 200 μm.

Error bars represent mean ± SEM. *= p<0.05, **= p<0.01.

had increased islet density and islet area than in corresponding controls (Figure 7F). This observation extends recent findings that SCGN promotes islet integrity and β-cell mass (Malenczyk et al., 2017). The liver of untreated animals had prominent hepatic necrosis along with large fat bodies (as also visualized in Oil Red O-stained liver sections; Figure S9C), whereas treated animals were largely protected from necrosis and fat deposition. Because chronic metabolic stress leads to renal dysfunction, and the rSCGN administration was a relatively long-term study, we confirmed that excretory system is not stressed due to rSCGN administration. Consistently, due to long-term HFD-induced metabolic stress, kidneys of untreated HFD-fed animals were severely degenerated, with large necrotic areas devoid of cells. Glomerular density was also reduced in untreated HFD-fed animals. In rSCGN-treated animals, these features were less prominent, likely due to a reduced glycemic and metabolic load. These observations suggest that rSCGN administration not only improves glucose and lipid metabolism but also helps in maintaining the metabolic organs healthy.

## SCGN Administration Causes Pancreatic β-cell Regeneration

Based on our observations that rSCGN administration increases β-cell proliferation in HFD-fed animals, we wondered if it would exert a similar effect in the β-cell-deficient STZ animals. After four weeks of rSCGN injections (10 mg/kg, on alternate days), STZ mice had increased islet frequency and islet area in pancreatic sections (Figure 8A) when compared with control mice. Although it is not clear if exogenous SCGN mimics

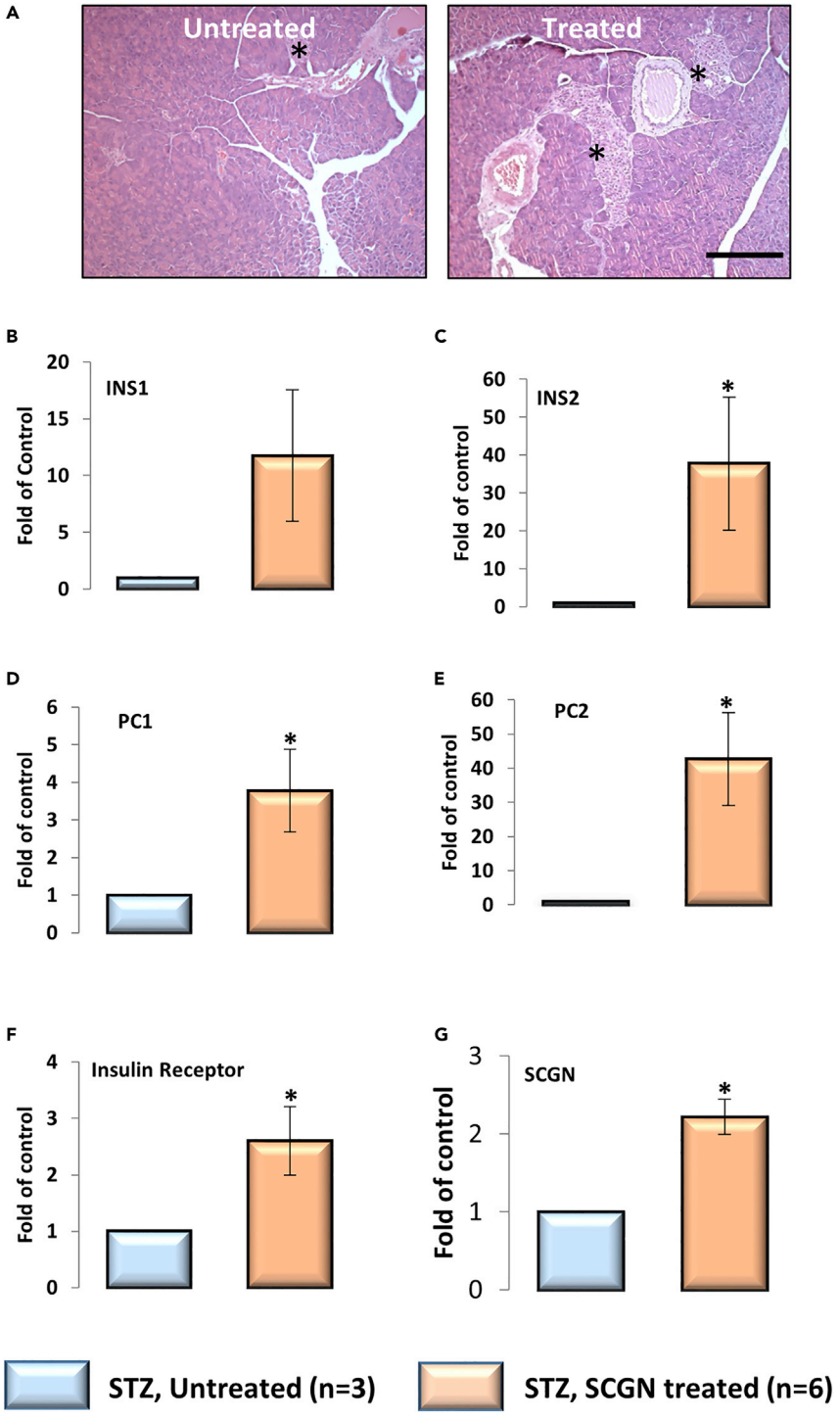


**Figure 8. SCGN-Induced Pancreatic β-cell Proliferation and Gene Expression in STZ Mice**

(A) H&E staining of formalin-fixed pancreas sections of STZ-treated BALB/c mice upon SCGN treatment. Scale bar, 200 μm.

(B–G) Transcriptional reprogramming of pancreatic genes in STZ-untreated and SCGN-treated animals as measured by qRT-PCR.

Error bars represent mean ± SEM. *= $p<0.05$.

endogenous molecular function in maintaining β-cell mass, or if it embraces a new pathway, our results suggest a prospective application of SCGN in β-cell regeneration. Although it is interesting to notice therapeutically relevant islet regenerative activity of SCGN, it will be useful to discern an active minimal peptide with enhanced efficacy and specificity at lower doses.

To validate if the enhanced islets in SCGN-treated STZ animals harbor functional β-cells, we characterized the molecular expression of β-cell-specific genes by qRT-PCR analysis (Figures 8B–8G). A substantial increase was seen in the expression of insulin-signaling-related genes in the pancreas, suggesting an increase in total β-cell mass. Both isoforms of insulin (*INS1* and *INS2*) were upregulated in the pancreas of rSCGN-treated animals, suggesting a true increase in β-cell content (Figures 8B and 8C). In addition, insulin receptor (*INSR*) and prohormone convertase (*PC1/3* and *PC2*) were significantly upregulated (Figures 8D–8F). Moreover, *SCGN* was also upregulated in treated animals (Figure 8G). Increased β-cell mass and enhanced insulin expression suggest that rSCGN treatment can increase the insulin-producing capacity of insulin-deficient animals, whereas increased IR expression provides a way to achieve increased insulin sensitivity. Prohormone convertase (PC1/3) has a critical role in insulin maturation, and its upregulation fulfills the obvious requirement of insulin maturation. Interestingly, PC2, which is primarily involved in glucagon maturation, was also upregulated in SCGN-treated animals. Although we did not explore the possibility, this suggests that SCGN's functional role may extend to α-cell biology and glucagon secretion from the pancreas. To establish the organ specificity of SCGN action on transcriptional modulation, we quantified the expression of authentic hepatic genes. Except insulin receptor (which was significantly upregulated), other tested genes' expression was unaltered (Figure S11), suggesting a tissue-specific modulation of specific genes by circulatory SCGN.

## DISCUSSION

Insulin, secreted from pancreatic β-cells, acts on several organs, such as liver, muscle, and fat tissue to maintain normoglycemia. To perform these functions, insulin travels long distances, encountering harsh, multicomponent circulatory environment, which occasionally causes aggregation of insulin leading to diabetes (Baker et al., 1988; Hua et al., 1996, 2002). Because insulin is a vulnerable hormone, it forms $Zn^{2+}$-mediated tetramer/hexamer to attain stability in pancreatic β-cells (Blundell et al., 1972, 1972a; Emdin et al., 1980). However, once the complex reaches the circulation, $Zn^{2+}$ dissociates from insulin, which returns to the monomeric, biologically active form. Undesirably, the monomeric insulin is more prone to aggregation, fibrillation, and other anomalies (Gold and Grodsky, 1984; Formby et al., 1984; Li, 2014; Robertson et al., 2011). These anomalies impose a fundamental question on insulin stabilization and add to pharmaceutical difficulties in insulin manufacture and therapy (Brange, 1987; Brange et al., 1997; Vajo et al., 2001). Insulin-like growth factors (IGFs) are insulin-related hormones with similar structural features but different functions. To regulate the function and half-life of IGFs, there is a dedicated family of proteins called IGFBPs (Clemmons, 1993; Bach, 2015). However, for insulin, despite being an important hormone of primary importance, a circulatory InsBP has not been identified. The aggregation-prone disposition of insulin intuitively necessitates a structural stabilizer while in circulation. Although earlier studies suggested the existence of cytosolic insulin-binding proteins (CIBP) (Harada et al., 1995, 1996; Lokhov et al., 2004), to the best of our knowledge, circulatory InsBP remain an abstract idea. Harada et al. (Harada et al., 1996), in addition to several other proteins, described a 32 kDa CIBP, which was found to interact with insulin in the serum or in insulin-treated cells but not in serum-deprived cells. Coincidentally, SCGN is a 32 kDa protein and has been shown to exhibit serum/insulin responsive expression (Maj et al., 2012), suggesting that the reported 32 kDa CIBP could be SCGN. Moreover, SCGN seems to be synchronously secreted with insulin upon cAMP stimulation (Gartner et al., 2007). Likewise, a measurable fraction of SCGN dwells in circulation (Gartner et al., 2001; Tan et al., 2012), but the biological functions and the insulin-binding propensity of SCGN remain unexplored. Based on these interesting possibilities and our pull-down results, we argued that, owing to its localization and secretory properties, SCGN ought to be a candidate protein acting as InsBP. Here, we report that SCGN is an InsBP.

Protein fibrillation (including that of insulin) is a prominent anomaly associated with diabetes and neurodegenerative diseases (Schneider et al., 1980; Maloy et al., 1981; Höppener et al., 2000; Ross and Poirier, 2004; Muchowski and Wacker, 2005; Wang et al., 2010). Insulin has been used as a model to study protein fibrillation *in vitro*. There are several macroscopic and microscopic mechanisms described for the formation of insulin fibrils (Hua and Weiss, 2004; Ivanova et al., 2009; Arosio et al., 2016). A prevailing model suggests that a well-folded insulin molecule, under amyloidogenic conditions, adopts a conformation of

protein-folding intermediate, which is prone to aggregation and self-association (Hua and Weiss, 2004). For chaperone-mediated protection of an amyloidogenic protein, it is suggested that although the microscopic mechanisms may differ from one chaperone/client to other, at macroscopic level chaperone proteins help a client protein to conserve its physiological, less aggregation-prone conformation (Arosio et al., 2016). In the case of SCGN-insulin, most plausible mechanism of protection is apparently the preservation of a soluble monomeric form where the aggregation-prone β-chain of insulin is protected by SCGN binding. This hypothesis is supported by the extended lag phase of insulin fibrillation as seen in ThT fluorescence and is also backed by the prevention of DTT-induced insulin aggregation, which directly indicates protection of β-chain of insulin. SCGN has earlier been reported to exert a possible protective effect against the Alzheimer disease (Attems et al., 2008; Maj et al., 2010) Thus, SCGN-mediated inhibition of fibrillation could provide a plausible explanation of the previously observed conspicuous protection against the disease. Moreover, it also suggests that SCGN is a common factor involved in diabetes and Alzheimer disease.

Besides exerting protection from fibrillation, SCGN also modulates insulin signaling. An SCGN-induced increase in insulin response in healthy animals prompted us to explore if the same would be true in diabetic animals as well. We found that prolonged SCGN treatment is required for sustained insulin sensitization and glucose lowering. The insulin dependence of SCGN action was further validated in STZ mice, a model for insulin deficiency. In both the animal models, we found that subcutaneous injection is more effective for sustained action when compared with intraperitoneal injection. We also studied the impact of rSCGN on hepatic fat deposition and degree of insulin resistance to discover the mechanism of sustained insulin sensitivity. Persistent hyperinsulinemia is directly implicated in obesity and insulin resistance (Pories and Dohm, 2012; Corkey, 2012; Vernochet et al., 2012; Pedersen et al., 2015; Templeman et al., 2015; D'souza et al., 2016). We observed that rSCGN treatment prevents hyperinsulinemia. Considering the previous findings that hyperinsulinemia is a crucial factor for the weight gain in DIO animals (Templeman et al., 2015; D'souza et al., 2016), reduced weight gain in SCGN-treated DIO animals is attributed to the reduction in hyperinsulinemia. Emerging evidence suggests that hepatic lipid accumulation is a prominent factor in insulin resistance and diabetes (Perry et al., 2014). We found that SCGN-administered animals had appreciably lower hepatic lipid accumulation, which conceivably is a consequence (and in a feedback loop, a contributor) of improved insulin sensitivity. The SCGN-mediated hepatic insulin clearance likely contributes to a reduction in circulating insulin levels and reduced weight gain in SCGN-treated DIO animals. Because diabetes is associated with increased risk of cardiovascular disease (Grundy et al., 1999; Resnick and Howard, 2002), the reduction of LDL by SCGN suggests that the SCGN administration could also reduce the risk of cardiac problems.

While examining the histological integrity of pancreas, liver, and kidney, we observed a positive systemic influence on key metabolic organs, which is ultimately reflected in better glycemic control in rSCGN-treated animals. In the backdrop of a recent study reporting the role of intracellular SCGN in maintaining β-cell mass (Malenczyk et al., 2017), our results showing that exogenous SCGN administration exerts a positive effect on islet regeneration are encouraging. These observations also corroborate with a recent study on the essentiality of SCGN for β-cell maturation and maintenance (Malenczyk et al., 2018). Moreover, owing to its insulin-sensitizing effect, SCGN emerges as a potential candidate against T2D. Future studies are needed to explore and optimize the therapeutic application of SCGN-induced β-cell regeneration. Being a relatively large protein, identifying individual domain(s) of SCGN responsible for specific function, such as β-cell regeneration or insulin sensitization, would be a fruitful exercise.

A recent report suggested that type 2 diabetes is a state of SCGN deficiency (Malenczyk et al., 2017). Similarly, *SCGN* knockout animals showed significant glucose intolerance (Malenczyk et al., 2017), pointing toward compromised insulin signaling. Our observations of synchronous secretion of SCGN and insulin compelled us to hypothesize that SCGN is a positive regulator of insulin action and this is why the SCGN knockout animals have compromised insulin function. Further, we demonstrate that exogenous SCGN supplementation can be used as preventive medicine in pre-diabetic animals. SCGN administration preserves insulin sensitivity and lowers systemic diabetes-associated complications in model systems. Thus, SCGN can also be used in combination with insulin (in type 1 diabetes) to increase insulin efficacy while promoting pancreatic regeneration over the course of treatment. Available anti-diabetic drugs have associated side effects such as weight gain, liver problems, and cardiovascular risk (Lehrke and Lazar,

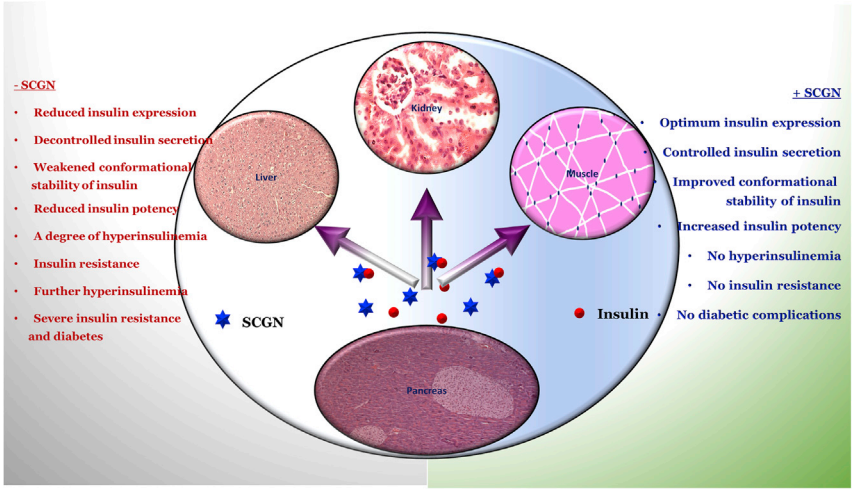


**Figure 9. Working Model**

SCGN positively regulates insulin expression and secretion (Wagner et al., 2000; Yang et al., 2016; Kobayashi et al., 2016). SCGN insulin interaction potentiates insulin stability and action and hence reducing the required effective concentration. Because increased circulatory insulin is also a founding factor for insulin resistance and diabetes, it suggests that insulin expression and functional regulation by SCGN is a mechanism for SCGN-mediated prevention of diabetes. The hypothesis is supported by a recent observation that the absence of SCGN leads to a compromised insulin action (Malenczyk et al., 2017).

2005; Stein et al., 2013; Inzucchi et al., 2014). In our study, we did not observe any prominent side effects even after five months of the rSCGN administration. Rather, rSCGN exerted beneficial effects, such as reduced serum $Ca^{2+}$, low-density lipoprotein, and hepatic steatosis.

In summary, our data establish SCGN as a functional insulin-binding protein. We demonstrate that insulin-binding ability bestows SCGN with competence to regulate the concentration, stability, and function of insulin beyond pancreas. As proposed recently (Sharma et al., 2019a, 2019b), SCGN administration potentially preserves insulin sensitivity and lowers systemic diabetes-associated complications in model systems (Figure 9). Thus, SCGN appears to be an effective preventive therapy against insulin resistance. Nonetheless, further work is required to derive mechanistic insights into the mode of action of SCGN and its potential use.

## Limitation of the Study

The physiological effect of exogenously SCGN administration on insulin action is examined in the HFD-fed wild-type mouse model. To discern the effect of exogenous SCGN from the endogenous SCGN, similar experiments carried out in SCGN knockout mouse model would provide further insight. It would not only validate the role of SCGN in diabetic pathophysiology but would also help in delineating the site of action of exogenous SCGN and provide mechanistic insight into pathways regulated by SCGN. Given the anticipated importance of SCGN in insulin potentiation, identifying the specific residues in the insulin-binding pocket of SCGN using NMR experiments would provide mechanistic insight and aid in developing the minimal SCGN peptide for potential therapeutic uses. Moreover, further studies with genetic models of diabetes are needed to derive mechanistic insight into the mode of SCGN action.

## Methods

All methods can be found in the accompanying Transparent Methods supplemental file.

## SUPPLEMENTAL INFORMATION

Supplemental Information can be found online at https://doi.org/10.1016/j.isci.2019.10.066.

## ACKNOWLEDGMENTS

Authors thank Miss Swathi Chadalawada for technical help. We are grateful to Drs. T Ramakrishna Murti and B Raman for help in biolayer interferometry. Mr Prashant and Mrs Jyothi have been helpful in a few animal experiments and Mr Harikrishna helped in TEM imaging. They thank Syed Sayeed Abdul for excellent laboratory assistance and Dr. Sushil Chandani for discussion and critical reading of the manuscript. In addition, discussions with Dr. G R Chandak were useful in experimental design. J. C Bose National Fellowship (SERB), CSIR, and DST are acknowledged for grants to Y.S.. H.C.A. and R.K. are the recipients of ICMR and CSIR-GATE research fellowships, respectively.

## AUTHOR CONTRIBUTIONS

Inception: A.K.S.; Experimental design: A.K.S., R.K., J.M.K., Y.S.; Protein purification: A.K.S., R.K., A.H.C.; Data acquisition: A.K.S., R.K., S.R.; Histology slide preparation: A.R.; Fibrillation experiments and TEM sample preparation: A.K.S., R.K., A.H.C.; Data analysis: A.K.S., R.K., J.M.K., Y.S.; Resources: Y.S.; Writing—original draft: A.K.S., R.K., Y.S.; Writing—review and editing: A.K.S., R.K., Y.S.; Supervision, project administration and funding acquisition: Y.S.

## DECLARATION OF INTERESTS

The authors declare that they have no conflict of interest with the content of this article. Current affiliation of AKS is Laboratory of Translational Nutrition Biology, DHEST, ETH Zurich (email id: anand.sharma@hest.ethz.ch).

Received: April 19, 2019
Revised: September 17, 2019
Accepted: October 29, 2019
Published: November 22, 2019

## REFERENCES

Arosio, P., Michaels, M.C.T., Linse, S., Månsson, C., Emanuelsson, C., Presto, J., Johansson, J., Vendruscolo, M., Dobson, C.M., and Knowles, T.P.J. (2016). Kinetic analysis reveals the diversity of microscopic mechanisms through which molecular chaperones suppress amyloid formation. Nat. Commun. *7*, 10948.

Attems, J., Preusser, M., Grosinger-Quass, M., Wagner, L., Lintner, F., and Jellinger, K. (2008). Calcium-binding protein secretagogin-expressing neurons in the human hippocampus are largely resistant to neurodegeneration in Alzheimer's disease. Neuropathol. Appl. Neurobiol. *34*, 23–32.

Baker, E.N., Blundell, T.L., Cutfield, J.F., Cutfield, S.M., Dodson, E.J., Dodson, G.G., Hodgkin, D.M., Hubbard, R.E., Isaacs, N.W., and Reynolds, C.D. (1988). The structure of 2Zn pig insulin crystals at 1.5 A resolution. Philos. Trans. R. Soc. Lond. B Biol. Sci. *319*, 369–456.

Bach, L.A. (2015). Insulin-like growth factor binding proteins–an update. Pediatr. Endocrinol. Rev. *13*, 521–530.

Becerra-Tomás, N., Estruch, R., Bulló, M., Casas, R., Díaz-López, A., Basora, J., Fitó, M., Serra-Majem, L., and Salas-Salvadó, J. (2014). Increased serum calcium levels and risk of type 2 diabetes in individuals at high cardiovascular risk. Diabetes Care *37*, 3084–3091.

Behan, D.P., De Souza, E.B., Lowry, P.J., Potter, E., Sawchenko, P., and Vale, W.W. (1995). Corticotropin releasing factor (CRF) binding protein: a novel regulator of CRF and related peptides. Front. Neuroendocrinol. *16*, 362–382.

Blundell, T.L., Cutfield, J.F., Cutfield, S.M., Dodson, E.J., Dodson, G.G., Hodgkin, D.C., and Mercola, D.A. (1972). Three-dimensional atomic structure of insulin and its relationship to activity. Diabetes *21*, 492–505.

Blundell, T.L., Cutfield, J.F., Dodson, E.J., Dodson, G.G., Hodgkin, D.C., and Mercola, D.A. (1972a). The crystal structure of rhombohedral 2 zinc insulin. Cold Spring Harb. Symp. Quant. Biol. *36*, 233–241.

Brange, J. (1987). Galenics of Insulin: The Physico-Chemical and Pharmaceutical Aspects of Insulin and Insulin Preparations (Springer-Verlag).

Brange, J., Andersen, L., Laursen, E.D., Meyn, G., and Rasmussen, E. (1997). Toward understanding insulin fibrillation. J. Pharm. Sci. *86*, 517–525.

Clemmons, D.R. (1993). IGF binding proteins and their functions. Mol. Reprod. Dev. *35*, 368–375.

Corkey, B.E. (2012). Banting lecture 2011: hyperinsulinemia: cause or consequence? Diabetes *61*, 4–13.

Czech, M.P. (2017). Insulin action and resistance in obesity and type 2 diabetes. Nat. Med *23*, 804–814.

D'souza, A.M., Johnson, J.D., Clee, S.M., and Kieffer, T.J. (2016). Suppressing hyperinsulinemia prevents obesity but causes rapid onset of diabetes in leptin-deficient Lepob/ob mice. Mol. Metab. *5*, 1103–1112.

Emdin, S.O., Dodson, G.G., Cutfield, J.M., and Cutfield, S.M. (1980). Role of zinc in insulin biosynthesis. Some possible zinc-insulin interactions in the pancreatic β-cell. Diabetologia *19*, 174–182.

Finn, T.E., Nunez, A.C., Sunde, M., and Easterbrook-Smith, S.B. (2012). Serum albumin prevents protein aggregation and amyloid formation and retains chaperone-like activity in the presence of physiological ligands. J. Biol. Chem. *287*, 21530–21540.

Formby, B., Schmid-Formby, F., and Grodsky, G.M. (1984). Relationship between insulin release and $^{65}$zinc efflux from rat pancreatic islets maintained in tissue culture. Diabetes *33*, 229–234.

Gartner, W., Lang, W., Leutmetzer, F., Domanovits, H., Waldhäusl, W., and Wagner, L. (2001). Cerebral expression and serum detectability of secretagogin, a recently cloned EF-hand $Ca^{2+}$-binding protein. Cereb. Cortex *11*, 1161–1169.

Gartner, W., Vila, G., Daneva, T., Nabokikh, A., Koc-Saral, F., Ilhan, A., Majdic, O., Luger, A., and Wagner, L. (2007). New functional aspects of the neuroendocrine marker secretagogin based on the characterization of its rat homolog. Am. J. Physiol. Endocrinol. Metab. *293*, 347–354.

Gold, G., and Grodsky, G.M. (1984). Kinetic aspects of compartmental storage and secretion of insulin and zinc. Experientia *40*, 1105–1114.

Grundy, S.M., Benjamin, I.J., Burke, G.L., Eckel, A.C.R.H., Howard, B.V., Mitch, W., Smith, S.C., and Sowers, J.R. (1999). Diabetes and

cardiovascular disease. Circulation *100*, 1134–1146.

Gutt, M., Davis, C.L., Spitzer, S.B., Llabre, M.M., Kumar, M., Czarnecki, E.M., Schneiderman, N., Skyler, J.S., and Marks, J.B. (2000). Validation of the insulin sensitivity index ($ISI_{(0,120)}$): comparison with other measures. Diabetes Res. Clin. Pract. *47*, 177–184.

Harada, S., Smith, R.M., Smith, J.A., Shah, N., and Jarett, L. (1995). Demonstration of specific insulin binding to cytosolic proteins in H35 hepatoma cells, rat liver and skeletal muscle. Biochem. J. *306*, 21–28.

Harada, S., Smith, R.M., Hu, D.Q., and Jarett, L. (1996). Dexamethasone inhibits insulin binding to insulin-degrading enzyme and cytosolic insulin-binding protein p82. Biochem. Biophys. Res. Commun. *218*, 154–158.

Hasegawa, K., Wakino, S., Kimoto, M., Minakuchi, H., Fujimura, K., Hosoya, K., Komatsu, M., Kaneko, Y., Kanda, T., Tokuyama, H., et al. (2013). The hydrolase DDAH2 enhances pancreatic insulin secretion by transcriptional regulation of secretagogin through a Sirt1-dependent mechanism in mice. FASEB J. *27*, 2301–2315.

Holmes, D. (2016). Adipose tissue: angiogenic factor regulates beiging. Nat. Rev. Endocrinol. *12*, 626.

Höppener, J.W.M., Ahrén, B., and Lips, C.J.M. (2000). Islet amyloid and type 2 diabetes mellitus. N. Engl. J. Med. *343*, 411–419.

Hua, Q.X., Hu, S.Q., Frank, B.H., Jia, W., Chu, Y.C., Wang, S.H., Burke, G.T., Katsoyannis, P.G., and Weiss, M.A. (1996). Mapping the functional surface of insulin by design: structure and function of a novel A-chain analogue. J. Mol. Biol. *264*, 390–403.

Hua, Q.X., Chu, Y.C., Jia, W., Phillips, N.F.B., Wang, R.Y., Katsoyannis, P.G., and Weiss, M.A. (2002). Mechanism of insulin chain combination. Asymmetric roles of A-chain alpha-helices in disulfide pairing. J. Biol. Chem. *277*, 43443–43453.

Hua, Q.X., and Weiss, M.A. (2004). Mechanism of insulin fibrillation: the structure of insulin under amyloidogenic conditions resembles a protein-folding intermediate. J. Biol. Chem. *279*, 21449–21460.

Inzucchi, S.E., Lipska, K.J., Mayo, H., Bailey, C.J., and McGuire, D.K. (2014). Metformin in patients with type 2 diabetes and kidney disease: a systematic review. JAMA *312*, 2668–2675.

Ivanova, M.I., Sievers, S.A., Sawaya, M.R., Wall, J.S., and Eisenberg, D. (2009). Molecular basis for insulin fibril assembly. Proc. Natl. Acad. Sci. USA *106*, 18990–18995.

Khandelwal, R., Sharma, A.K., Chadalawada, S., and Sharma, Y. (2017). Secretagogin is a redox-responsive $Ca^{2+}$ sensor. Biochemistry *56*, 411–420.

Kobayashi, M., Yamato, E., Tanabe, K., Tashiro, F., Miyazaki, S., and Miyazaki, J. (2016). Functional analysis of novel candidate regulators of insulin secretion in the MIN6 mouse pancreatic β cell line. PLoS One *11*, e0151927.

Lehrke, M., and Lazar, M.A. (2005). The many faces of PPARγ. Cell *123*, 993–999.

Li, Y.V. (2014). Zinc and insulin in pancreatic beta-cells. Endocrine *45*, 178.

Lokhov, P.G., Moshkovskii, S.A., Ipatova, O.M., and Prozorovskii, V.N. (2004). Cytosolic insulin-binding proteins of mouse liver cells. Protein Pept. Lett. *11*, 29–33.

Maj, M., Gartner, W., Ilhan, A., Neziri, D., Attems, J., and Wagner, L. (2010). Expression of TAU in insulin-secreting cells and its interaction with the calcium-binding protein secretagogin. J. Endocrinol. *205*, 25–36.

Maj, M., Milenkovic, I., Bauer, J., Berggård, T., Veit, M., Ilhan-Mutlu, A., Wagner, L., and Tretter, V. (2012). Novel insights into the distribution and functional aspects of the calcium binding protein Secretagogin from studies on rat brain and primary neuronal cell culture. Front. Mol. Neurosci. *5*, 84.

Malenczyk, K., Girach, F., Szodorai, E., Storm, P., Segerstolpe, Å., Tortoriello, G., Schnell, R., Mulder, J., Romanov, R.A., Borók, E., et al. (2017). A TRPV1-to-secretagogin regulatory axis controls pancreatic β-cell survival by modulating protein turnover. EMBO J. *36*, 2107–2125.

Malenczyk, K., Szodorai, E., Schnell, R., Lubec, G., Szabó, G., Hökfelt, T., and Harkany, T. (2018). Secretagogin protects Pdx1 from proteasomal degradation to control a transcriptional program required for ß cell specification. Mol. Metab. *14*, 108–120.

Maloy, A.L., Longnecker, D.S., and Greenberg, E.R. (1981). The relation of islet amyloid to the clinical type of diabetes. Hum. Pathol. *12*, 917–922.

Muchowski, P.J., and Wacker, J.L. (2005). Modulation of neurodegeneration by molecular chaperones. Nat. Rev. Neurosci. *6*, 11–22.

Pedersen, D.J., Guilherme, A., Danai, L.V., Heyda, L., Matevossian, A., Cohen, J., Nicoloro, S.M., Straubhaar, J., Noh, H.L., Jung, D., et al. (2015). A major role of insulin in promoting obesity-associated adipose tissue inflammation. Mol. Metab. *4*, 507–518.

Perry, R.J., Samuel, V.T., Petersen, K.F., and Shulman, G.I. (2014). The role of hepatic lipids in hepatic insulin resistance and type 2 diabetes. Nature *510*, 84–91.

Pories, W.J., and Dohm, G.L. (2012). Diabetes: have we got it all wrong? Hyperinsulinism as the culprit: surgery provides the evidence. Diabetes Care *35*, 2438–2442.

Resnick, H.E., and Howard, B.V. (2002). Diabetes and cardiovascular disease. Annu. Rev. Med. *53*, 245–267.

Robertson, R.P., Zhou, H., and Slucca, M. (2011). A role for zinc in pancreatic islet beta-cell cross-talk with the alpha-cell during hypoglycaemia. Diabetes Obes. Metab. *13*, 106–111.

Rogstam, A., Linse, S., Lindqvist, A., James, P., Wagner, L., and Berggård, T. (2007). Binding of calcium ions and SNAP-25 to the hexa EF-hand protein secretagogin. Biochem. J. *401*, 353–363.

Rooney, M.R., Pankow, J.S., Sibley, S.D., Selvin, E., Reis, J.P., Michos, E.D., and Lutsey, P.L. (2016). Serum calcium and incident type 2 diabetes: the Atherosclerosis risk in communities (ARIC) study. Am. J. Clin. Nutr. *104*, 1023–1029.

Ross, C.A., and Poirier, M.A. (2004). Protein aggregation and neurodegenerative disease. Nat. Med *10*, S10–S17.

Samuel, V.T., and Shulman, G.I. (2012). Mechanisms for insulin resistance: common threads and missing links. Cell *148*, 852–871.

Schneider, H.M., Störkel, F.S., and Will, W. (1980). The influence of insulin on local amyloidosis of the islets of Langerhans and insulinoma. Pathol. Res. Pract. *170*, 180–191.

Schneidman-Duhovny, D., Inbar, Y., Nussinov, R., and Wolfson, H.J. (2005). PatchDock and SymmDock: servers for rigid and symmetric docking. Nucleic Acids Res. *33*, W363–W367.

Sharma, A.K., Khandelwal, R., and Sharma, Y. (2019a). Veiled potential of secretagogin in diabetes: correlation or coincidence? Trends Endocrinol. Metab. *30*, 234–243.

Sharma, A.K., Khandelwal, R., and Sharma, Y. (2019b). Secretagogin purification and quality control strategies for biophysical and cell biological studies. Methods Mol. Biol. *1929*, 551–566.

Sharma, A.K., Khandelwal, R., Sharma, Y., and Rajnikanth, V. (2015). Secretagogin, a hexa EF-hand CaBP: high level, one-step bacterial purification, and properties. Protein Expr. Purif. *109*, 113–119.

Stein, S.A., Lamos, E.M., and Davis, S.N. (2013). A review of the efficacy and safety of oral antidiabetic drugs. Expert Opin. Drug Saf. *12*, 153–175.

Tan, W.S., Lee, J.J., Satish, R.L., and Ang, E.T. (2012). Detectability of secretagogin in human erythrocytes. Neurosci. Lett. *526*, 59–62.

Templeman, N.M., Clee, S.M., and Johnson, J.D. (2015). Suppression of hyperinsulinaemia in growing female mice provides long-term protection against obesity. Diabetologia *58*, 2392–2402.

Thalassinos, N.C., Hadjiyanni, P., Tzanela, M., Alevizaki, C., and Philokiprou, D. (1993). Calcium metabolism in diabetes mellitus: effect of improved blood glucose control. Diabet. Med. *10*, 341–344.

Vernochet, C., Mourier, A., Bezy, O., Macotela, Y., Boucher, J., Rardin, M.J., An, D., Lee, K.Y., Ilkayeva, O.R., Zingaretti, C.M., et al. (2012). Adipose-specific deletion of TFAM increases mitochondrial oxidation and protects mice against obesity and insulin resistance. Cell Metab. *16*, 765–776.

Van Gaal, L.F., Mertens, I.L., and De Block, C.E. (2006). Mechanisms linking obesity with cardiovascular disease. Nature *444*, 875–880.

Vajo, Z., Fawcett, J., and Duckworth, W.C. (2001). Recombinant DNA technology in the treatment of diabetes: insulin analogs. Endocr. Rev. *22*, 706–717.

Wagner, L., Oliyarnyk, O., Gartner, W., Nowotny, P., Groeger, M., Kaserer, K., Waldhausl, W., and Pasternack, M.S. (2000). Cloning and expression of secretagogin, a novel neuroendocrine- and pancreatic islet of Langerhans-specific $Ca^{2+}$-binding protein. J. Biol. Chem. *75*, 24740–24751.

Wang, S.S., Liu, K.N., and Han, T.C. (2010). Amyloid fibrillation and cytotoxicity of insulin are inhibited by the amphiphilic surfactants. Biochim. Biophys. Acta *1802*, 519–530.

Westwood, S., Liu, B., Baird, A.L., Anand, S., Nevado-Holgado, A.J., Newby, D., Pikkarainen, M., Hallikainen, M., Kuusisto, J., Streffer, J.R., et al. (2017). The influence of insulin resistance on cerebrospinal fluid and plasma biomarkers of Alzheimer's pathology. Alzheimers Res. Ther. *9*, 31.

Yang, S.Y., Lee, J.J., Lee, J.H., Lee, K., Oh, S.H., Lim, Y.M., Lee, M.S., and Lee, K.J. (2016). Secretagogin affects insulin secretion in pancreatic β-cells by regulating actin dynamics and focal adhesion. Biochem. J. *473*, 1791–1803.

**ISCI, Volume *21***

## Supplemental Information

# Secretagogin Regulates Insulin Signaling by Direct Insulin Binding

**Anand Kumar Sharma, Radhika Khandelwal, M. Jerald Mahesh Kumar, N. Sai Ram, Amrutha H. Chidananda, T. Avinash Raj, and Yogendra Sharma**

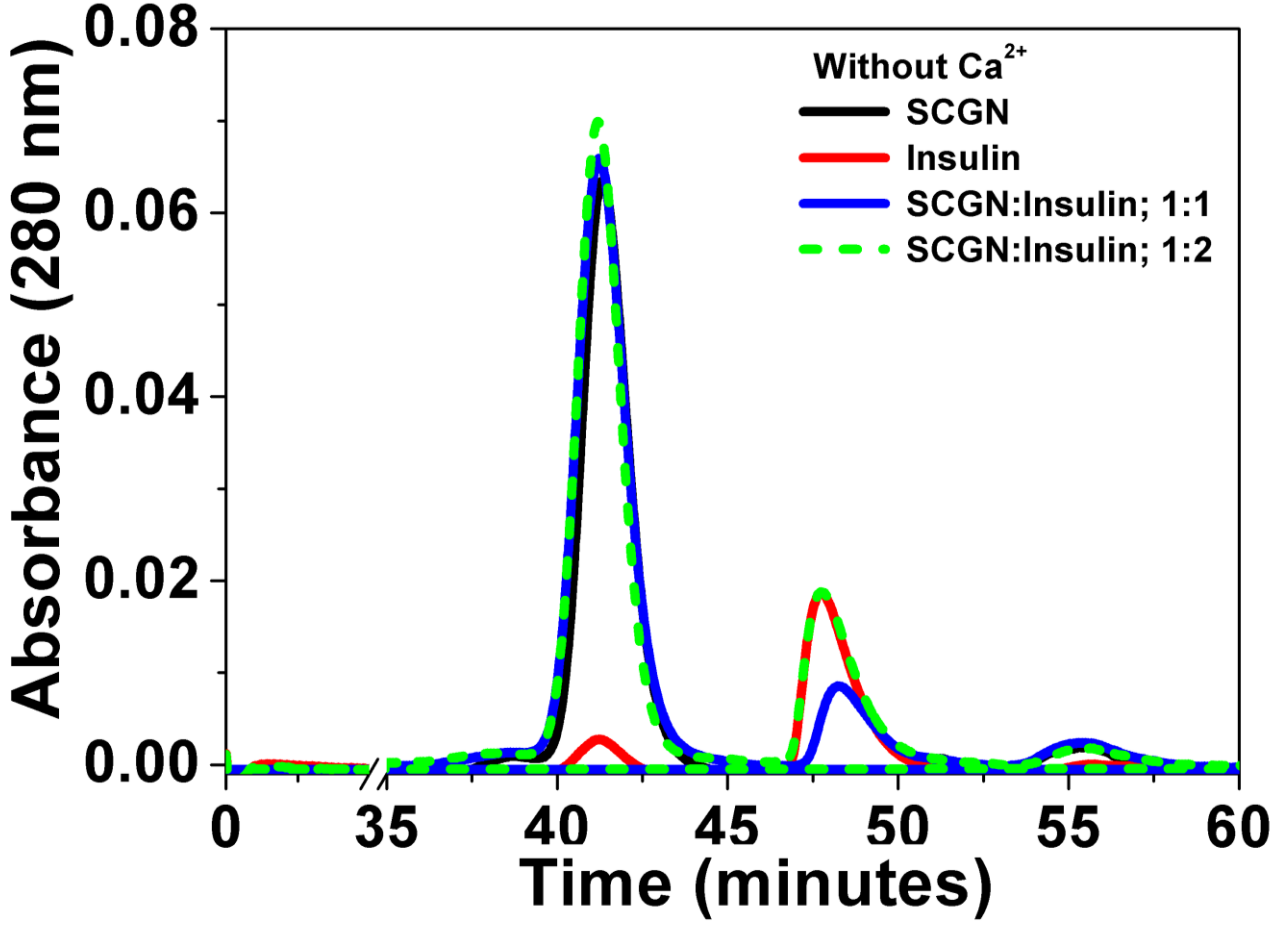
Without Ca2+
SCGN
Insulin
SCGN:Insulin; 1:1
SCGN:Insulin; 1:2
Absorbance (280 nm)
0.08
0.06
0.04
0.02
0.00
0
35
40
45
50
55
60
Time (minutes)

Fig. S1

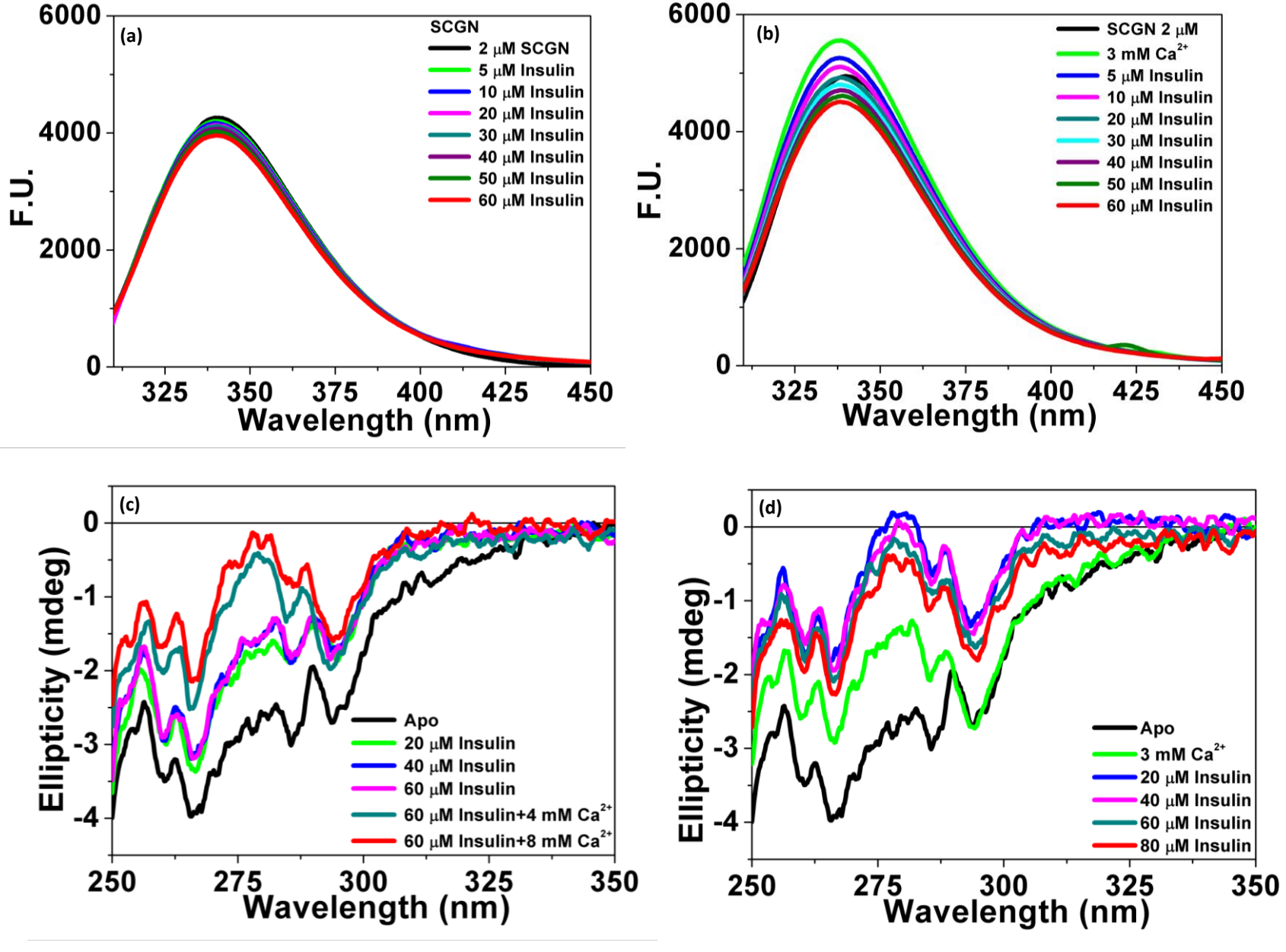
(a)
SCGN
2 μM SCGN
5 μM Insulin
10 μM Insulin
20 μM Insulin
30 μM Insulin
40 μM Insulin
50 μM Insulin
60 μM Insulin
F.U.
Wavelength (nm)
(b)
SCGN 2 μM
3 mM Ca2+
5 μM Insulin
10 μM Insulin
20 μM Insulin
30 μM Insulin
40 μM Insulin
50 μM Insulin
60 μM Insulin
F.U.
Wavelength (nm)
(c)
Apo
20 μM Insulin
40 μM Insulin
60 μM Insulin
60 μM Insulin+4 mM Ca2+
60 μM Insulin+8 mM Ca2+
Ellipticity (mdeg)
Wavelength (nm)
(d)
Apo
3 mM Ca2+
20 μM Insulin
40 μM Insulin
60 μM Insulin
80 μM Insulin
Ellipticity (mdeg)
Wavelength (nm)

**Fig. S2**

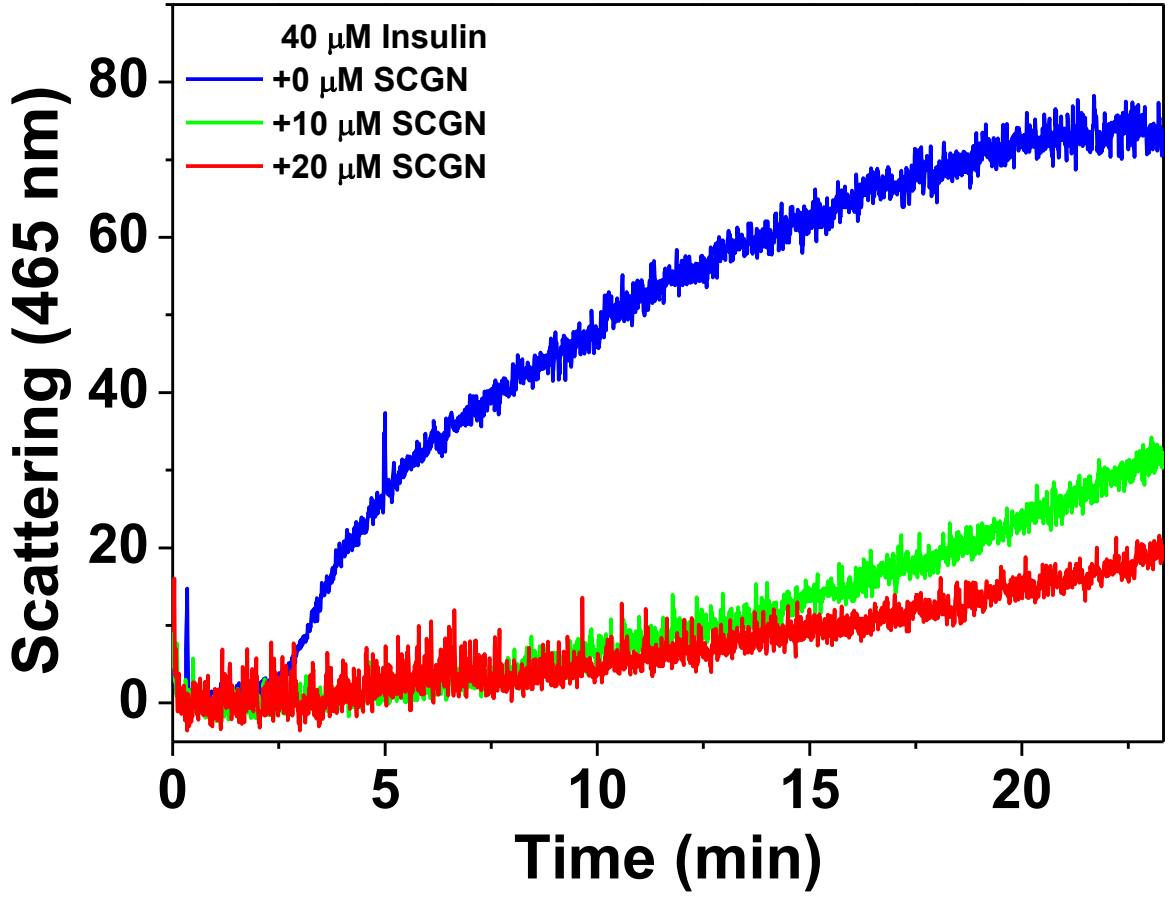
40 μM Insulin
+0 μM SCGN
+10 μM SCGN
+20 μM SCGN
Scattering (465 nm)
0
20
40
60
80
0
5
10
15
20
Time (min)

Fig. S3

## Differentiated C2C12 myotubes

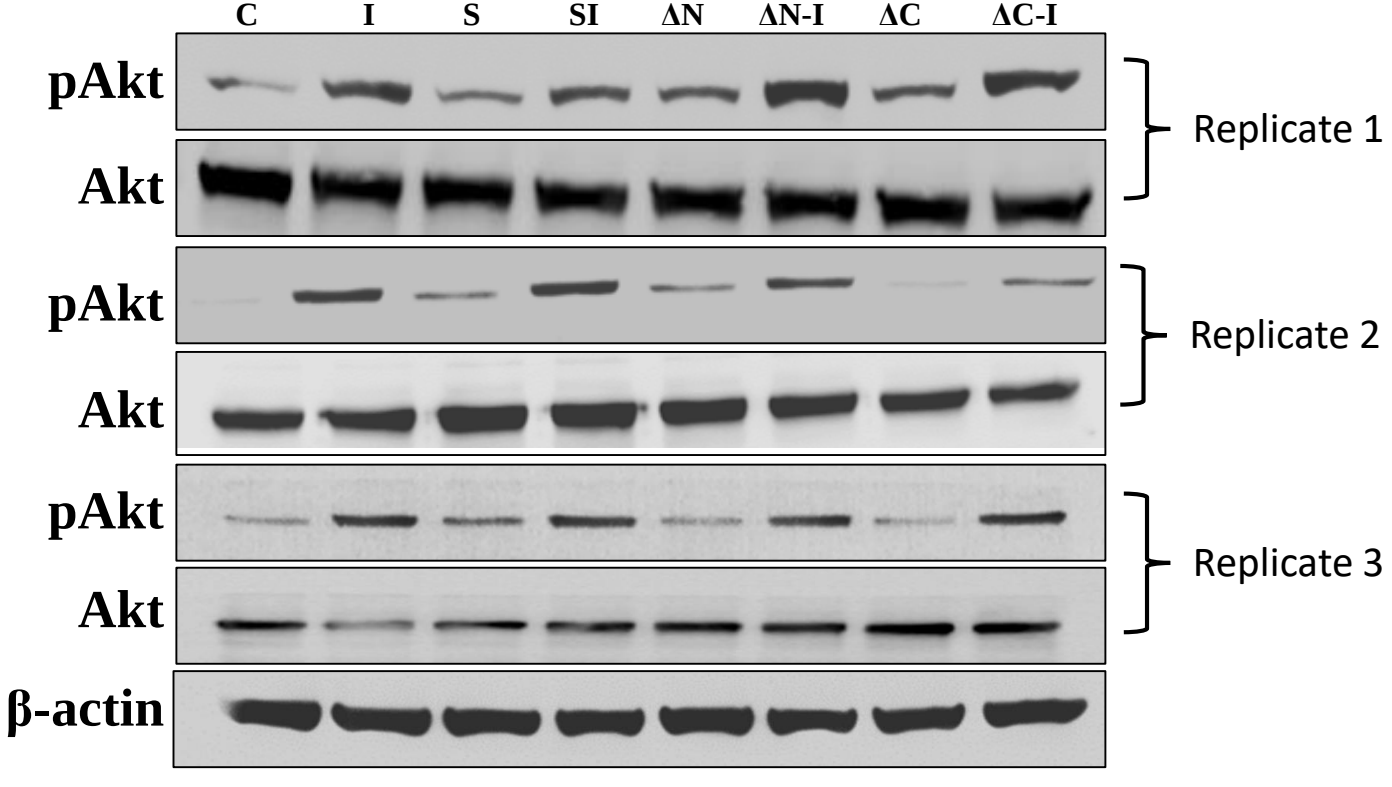


Fig. S4

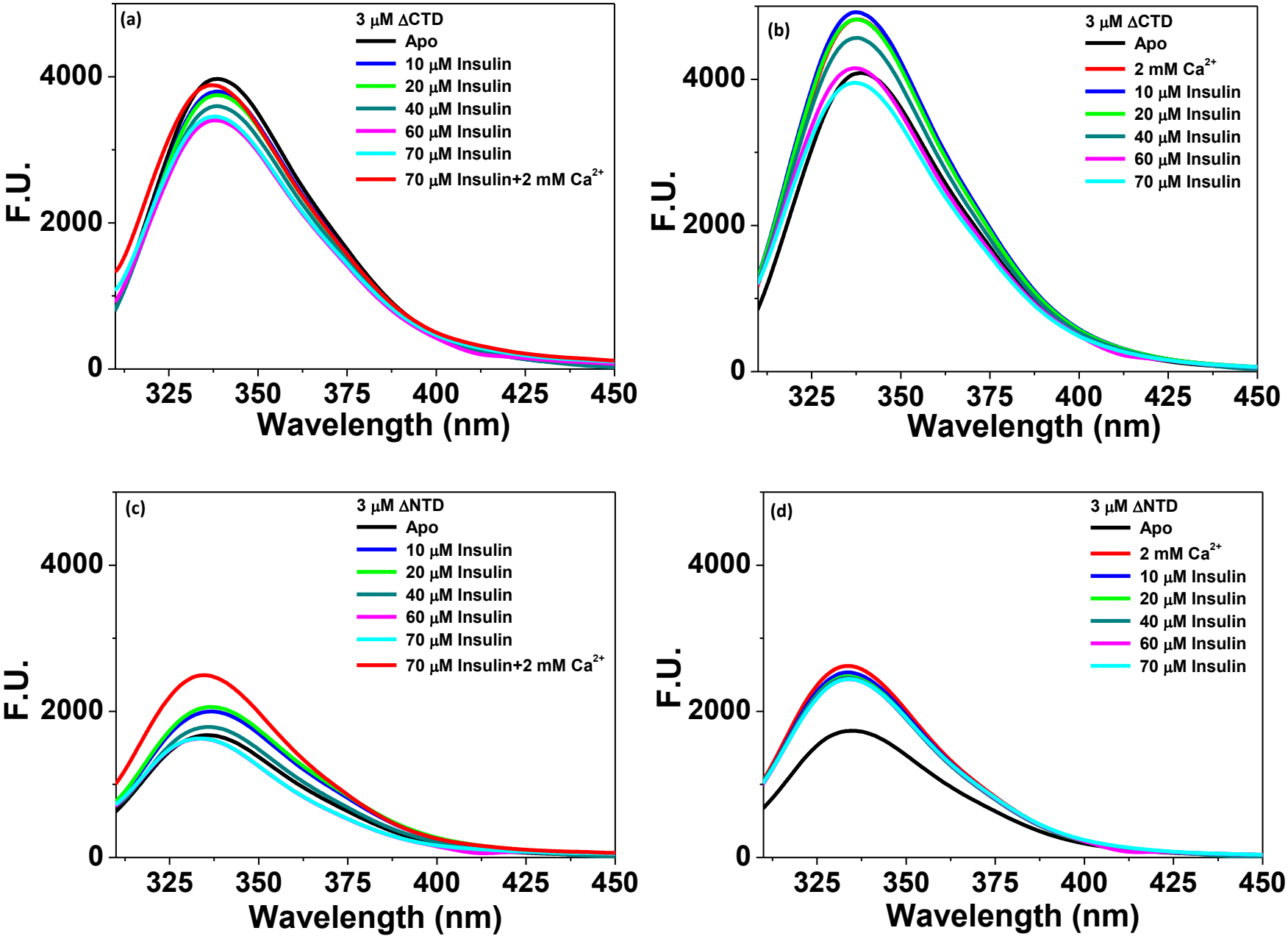
(a)
3 μM ΔCTD
Apo
10 μM Insulin
20 μM Insulin
40 μM Insulin
60 μM Insulin
70 μM Insulin
70 μM Insulin+2 mM Ca2+
F.U.
Wavelength (nm)
(b)
3 μM ΔCTD
Apo
2 mM Ca2+
10 μM Insulin
20 μM Insulin
40 μM Insulin
60 μM Insulin
70 μM Insulin
F.U.
Wavelength (nm)
(c)
3 μM ΔNTD
Apo
10 μM Insulin
20 μM Insulin
40 μM Insulin
60 μM Insulin
70 μM Insulin
70 μM Insulin+2 mM Ca2+
F.U.
Wavelength (nm)
(d)
3 μM ΔNTD
Apo
2 mM Ca2+
10 μM Insulin
20 μM Insulin
40 μM Insulin
60 μM Insulin
70 μM Insulin
F.U.
Wavelength (nm)

Fig. S5

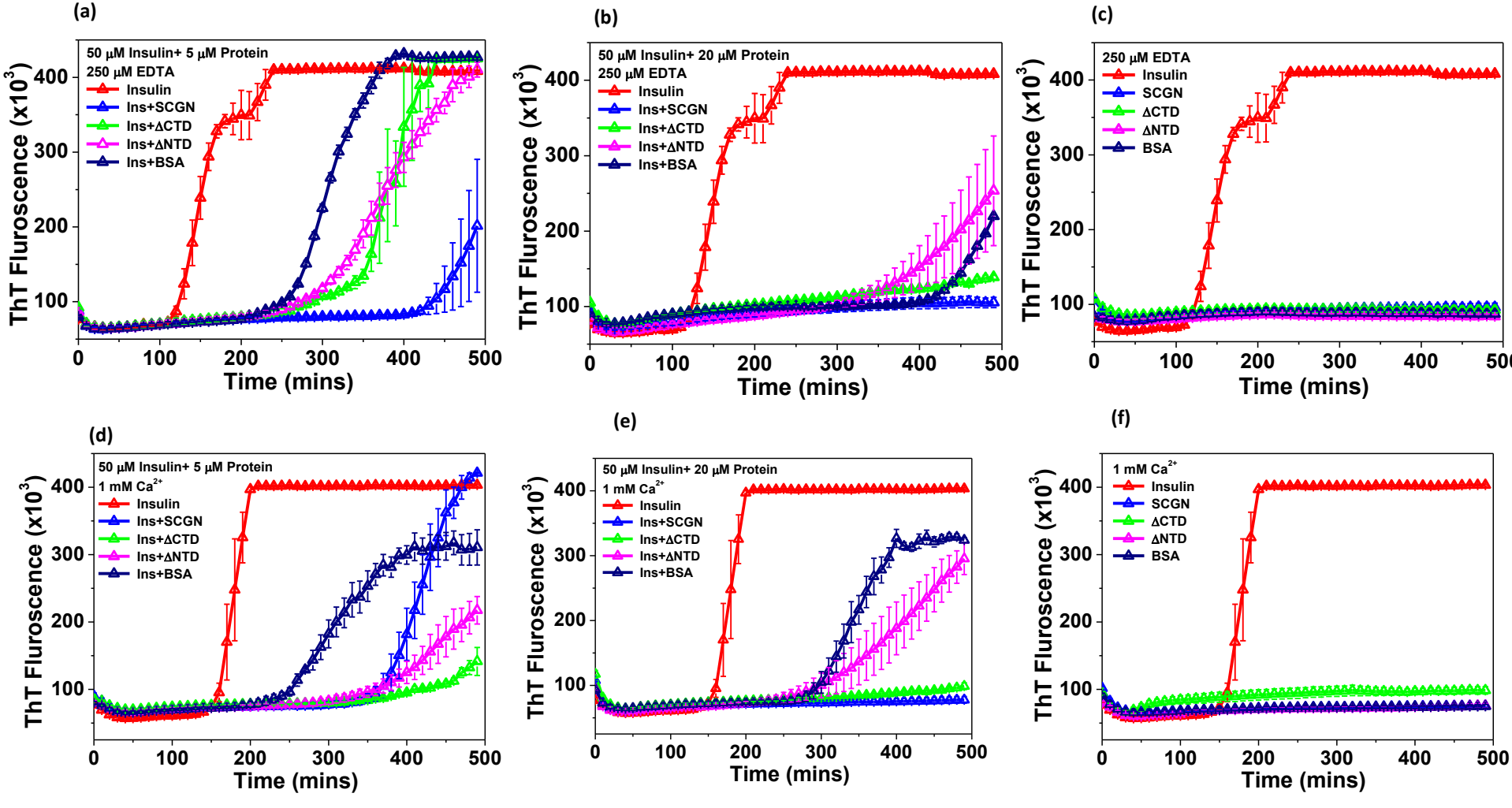
(a)
50 μM Insulin+ 5 μM Protein
250 μM EDTA
Insulin
Ins+SCGN
Ins+ΔCTD
Ins+ΔNTD
Ins+BSA
ThT Fluroscence (x10^3)
Time (mins)
(b)
50 μM Insulin+ 20 μM Protein
250 μM EDTA
Insulin
Ins+SCGN
Ins+ΔCTD
Ins+ΔNTD
Ins+BSA
ThT Fluroscence (x10^3)
Time (mins)
(c)
250 μM EDTA
Insulin
SCGN
ΔCTD
ΔNTD
BSA
ThT Fluroscence (x10^3)
Time (mins)
(d)
50 μM Insulin+ 5 μM Protein
1 mM Ca2+
Insulin
Ins+SCGN
Ins+ΔCTD
Ins+ΔNTD
Ins+BSA
ThT Fluroscence (x10^3)
Time (mins)
(e)
50 μM Insulin+ 20 μM Protein
1 mM Ca2+
Insulin
Ins+SCGN
Ins+ΔCTD
Ins+ΔNTD
Ins+BSA
ThT Fluroscence (x10^3)
Time (mins)
(f)
1 mM Ca2+
Insulin
SCGN
ΔCTD
ΔNTD
BSA
ThT Fluroscence (x10^3)
Time (mins)

Fig. S6

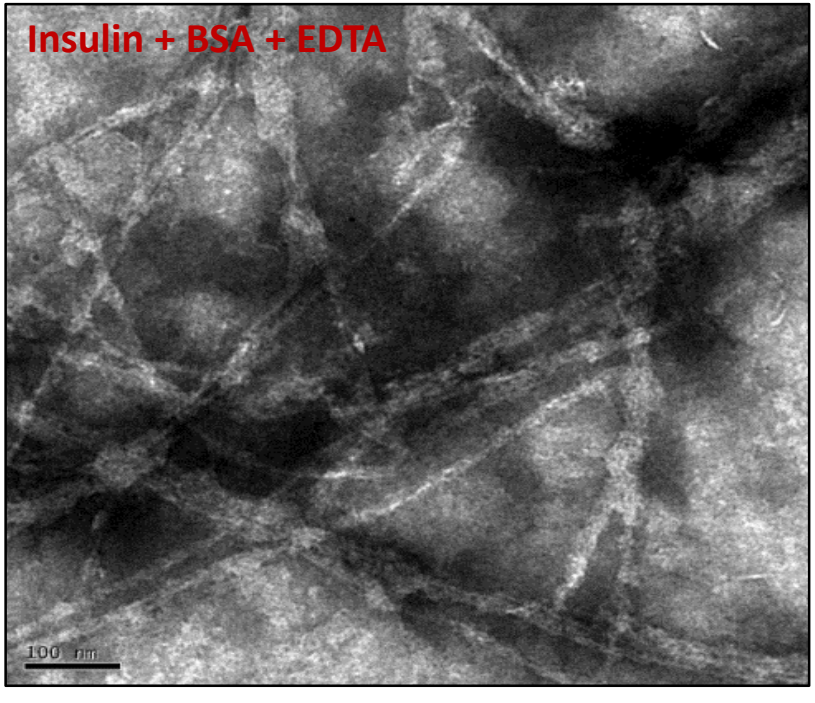


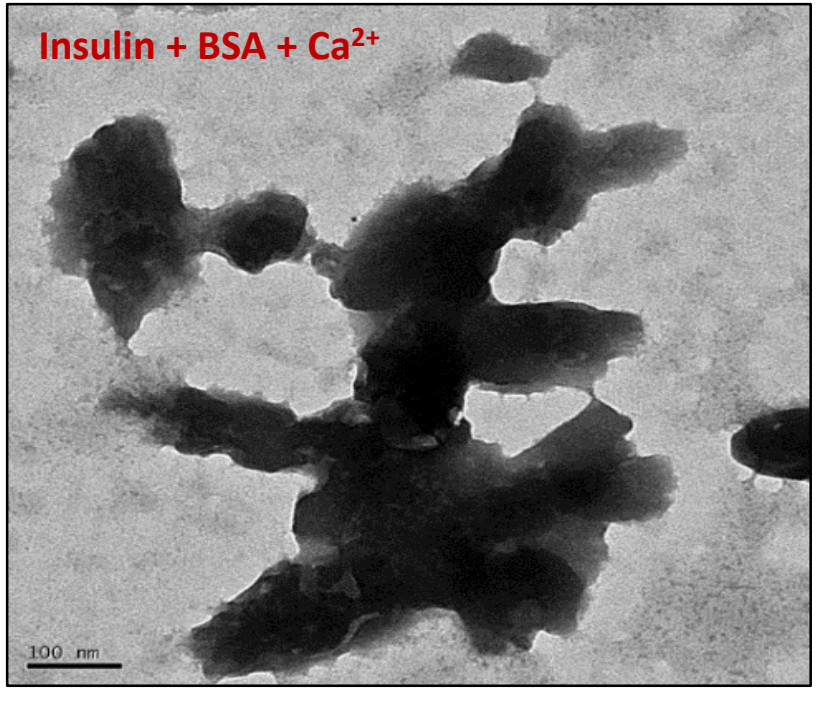


**Fig. S7**

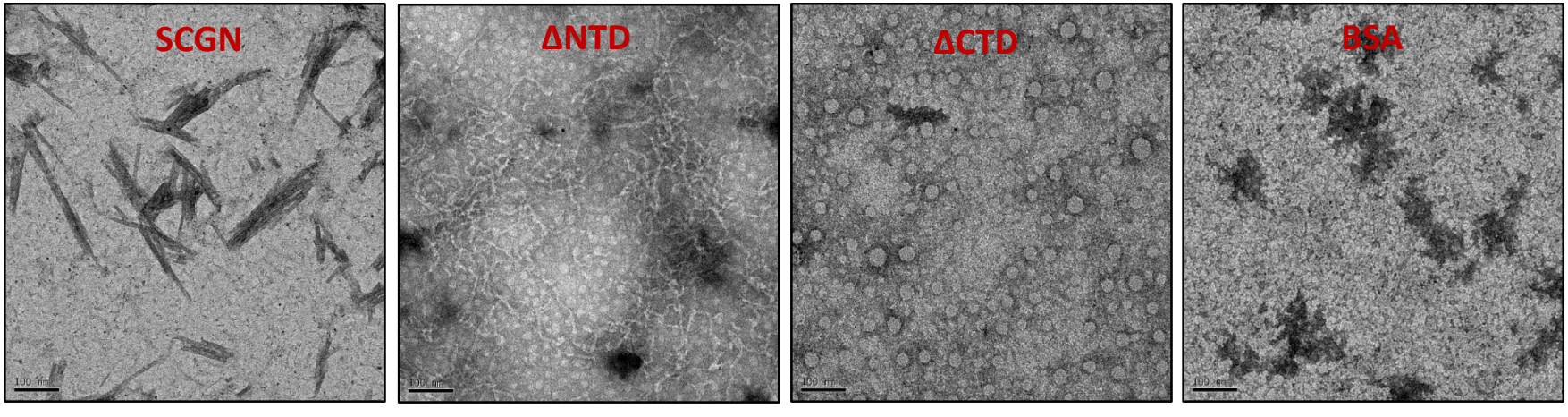


Fig. S8

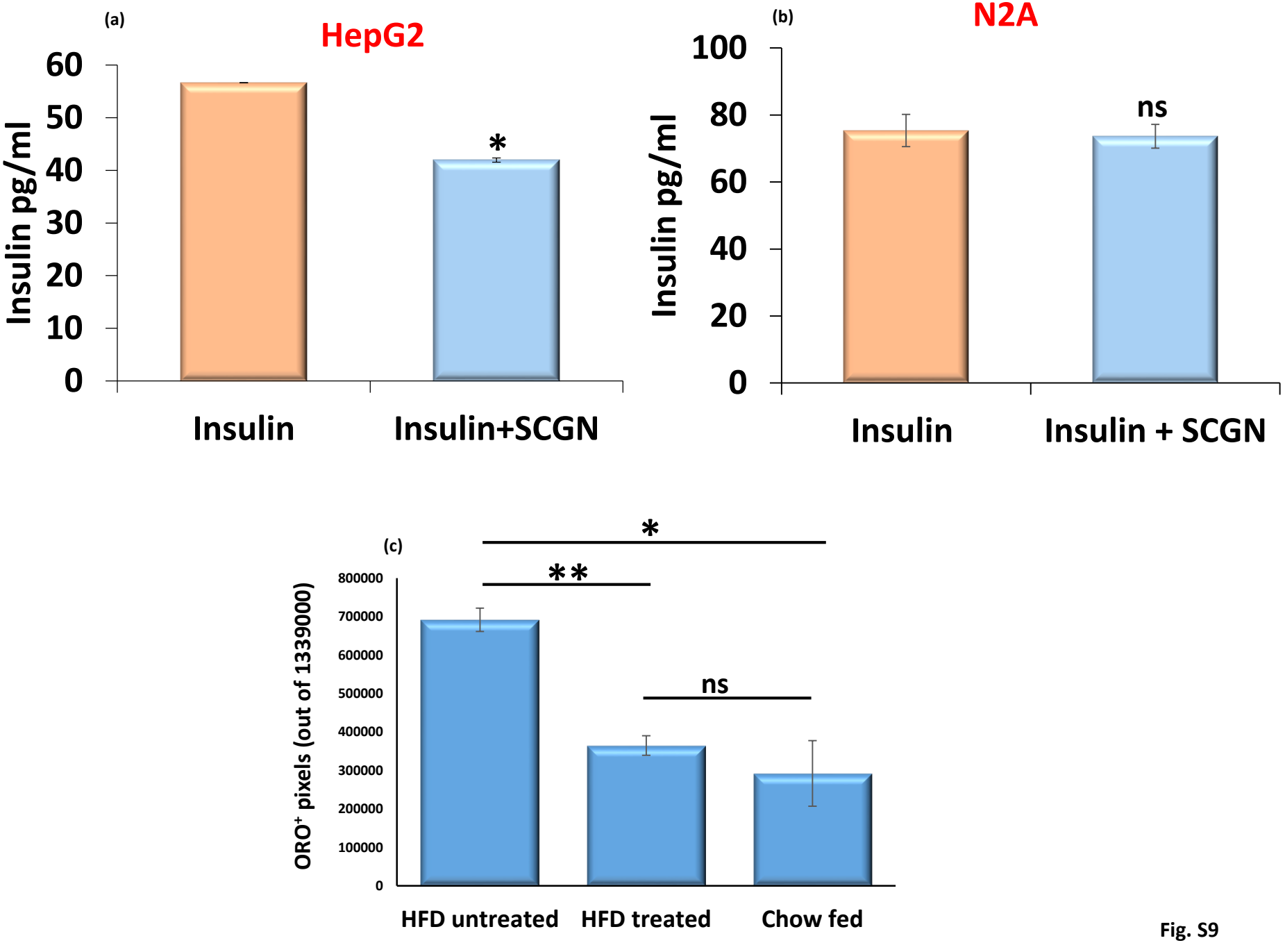
(a)
HepG2
Insulin pg/ml
60
50
40
30
20
10
0
*
Insulin
Insulin+SCGN
(b)
N2A
Insulin pg/ml
100
80
60
40
20
0
ns
Insulin
Insulin + SCGN
(c)
*
**
ns
ORO+ pixels (out of 1339000)
800000
700000
600000
500000
400000
300000
200000
100000
0
HFD untreated
HFD treated
Chow fed

Fig. S9

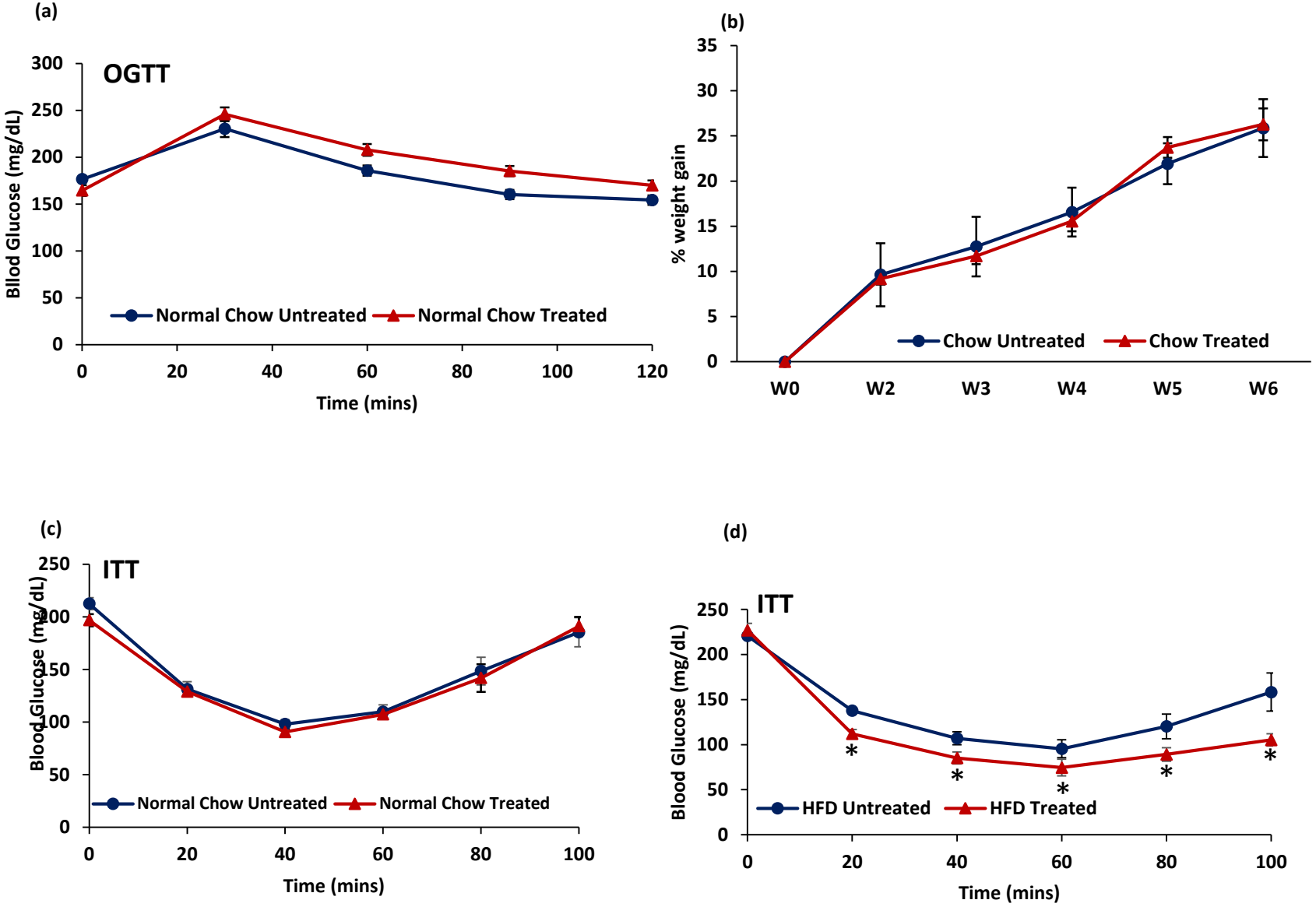
(a)
OGTT
Bllod Glucose (mg/dL)
300
250
200
150
100
50
0
0
20
40
60
80
100
120
Time (mins)
Normal Chow Untreated
Normal Chow Treated
(b)
% weight gain
35
30
25
20
15
10
5
0
W0
W2
W3
W4
W5
W6
Chow Untreated
Chow Treated
(c)
ITT
Blood Glucose (mg/dL)
250
200
150
100
50
0
0
20
40
60
80
100
Time (mins)
Normal Chow Untreated
Normal Chow Treated
(d)
ITT
Blood Glucose (mg/dL)
250
200
150
100
50
0
0
20
40
60
80
100
Time (mins)
HFD Untreated
HFD Treated
*
*
*
*
*

Fig. S10

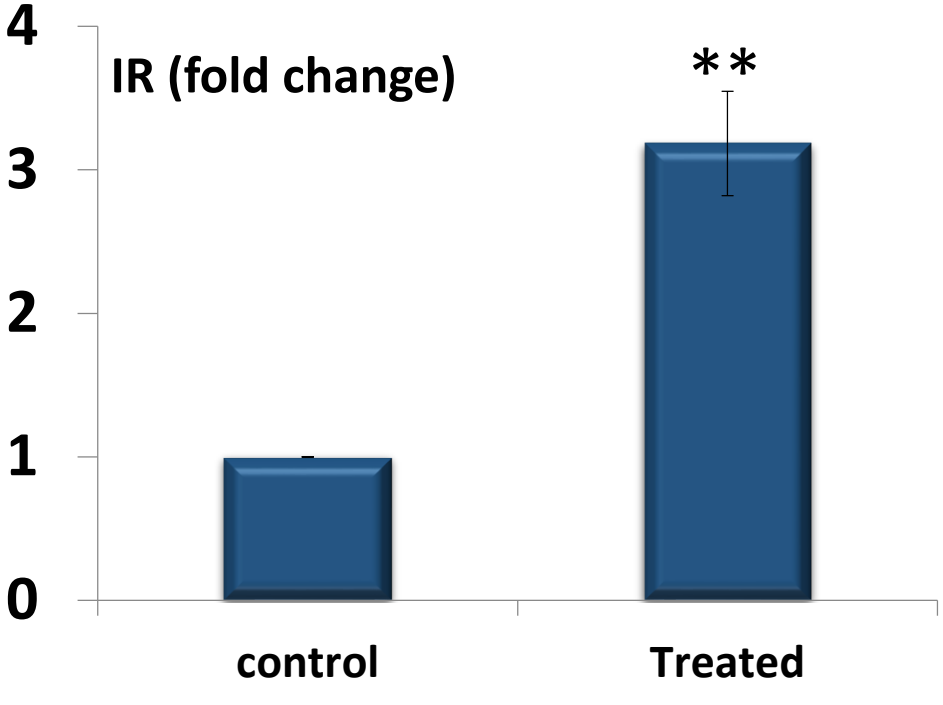


## Hepatic Genes Showing unperturbed expression

- ✓ FASN
- ✓ GlucoK
- ✓ G6Pase
- ✓ Glut4
- ✓ PEPCK
- ✓ SREB1
- ✓ p85a

Fig. S11

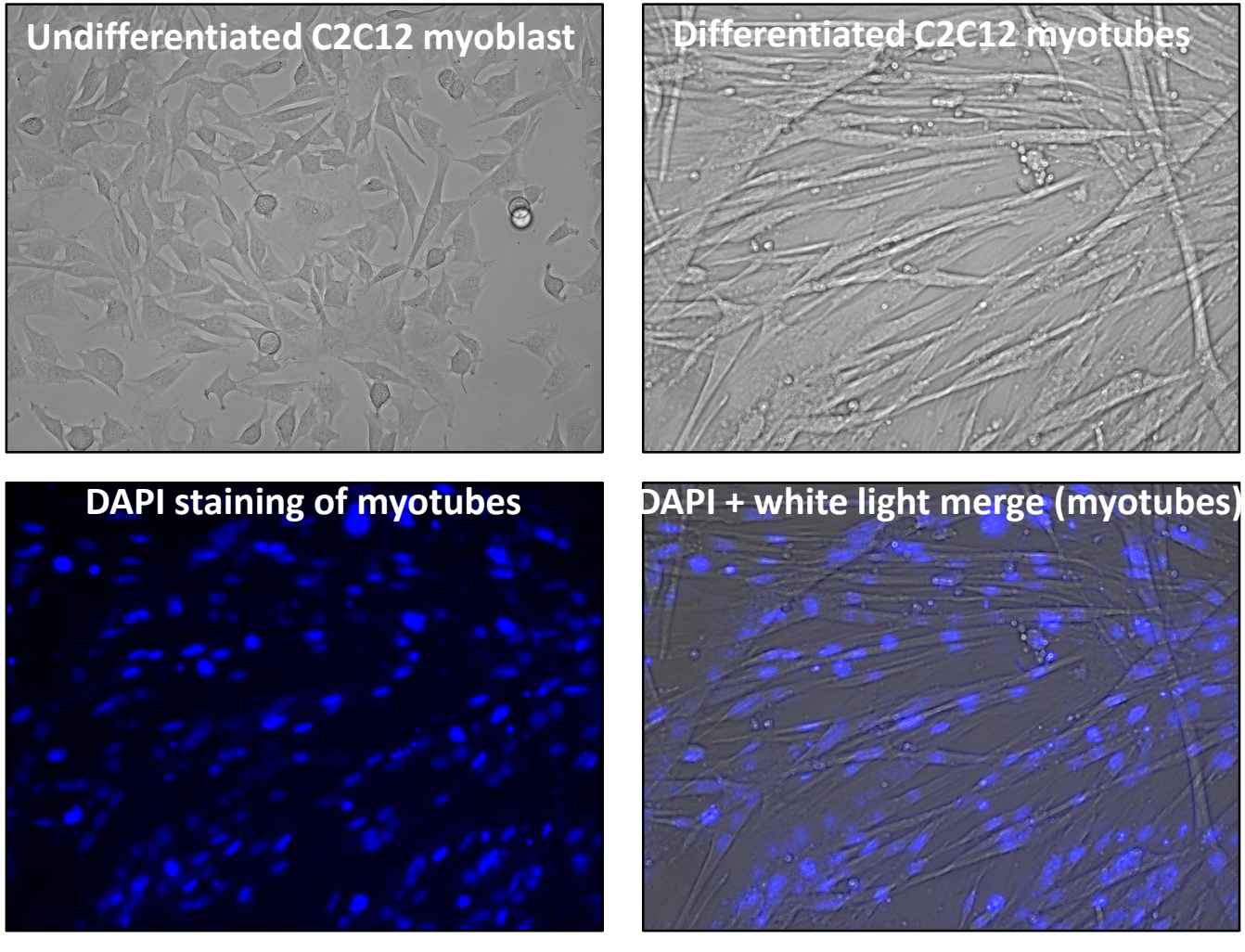
Undifferentiated C2C12 myoblast
Differentiated C2C12 myotubes
DAPI staining of myotubes
DAPI + white light merge (myotubes)

**Fig. S12**

## Supplementary figure legends

**Figure S1. Lack of stability of SCGN-insulin complex in the absence of $Ca^{2+}$, related to Figure 1.** Analytical gel filtration elution profile of individual proteins and SCGN-insulin mixture.

**Figure S2. $Ca^{2+}$ is a positive allosteric modulator of insulin binding to SCGN, related to Figure 1.** (a, b) fluorescence spectra demonstrating changes in Trp microenvironment of SCGN upon insulin titration into the apo- and holo-proteins; (c, d) Near UV-CD spectra of apo- and holo-SCGN upon insulin binding illustrating global conformational changes in the protein.

**Figure S3. SCGN protects insulin from DTT induced aggregation, related to Figure 2.** Change in Rayleigh scattering demonstrating the extent of insulin aggregation upon addition of DTT in the presence or absence of SCGN.

**Figure S4. Central domain of SCGN modulates *in vitro* insulin response, related to Figure 4.** C2C12 cells were treated with given protein/insulin combinations and Akt phosphorylation was assessed with pAkt specific antibody. Note a minimal effect of terminal-domains truncation on insulin potentiation suggesting that the central domain may have a role in modulating insulin activity *in vitro*.

**Figure S5. N-terminal domain deletion impedes insulin binding, related to Figure 4.** (a-d) Fluorescence spectra demonstrating changes in Trp microenvironment of truncated SCGN upon insulin titration into the apo- and holo-ΔCTD (a, b) or apo- and holo-ΔNTD (c, d). There was an appreciable reduction in insulin-induced fluorescence changes in ΔNTD.

**Figure S6. N-terminal domain deletion leads to compromised insulin protection, related to Figure 4. (a-c: $Ca^{2+}$ free conditions/d-f: $Ca^{2+}$ rich condition)**. (a, b, d, e) In Insulin fibrillation as monitored by ThT dye at given protein/insulin concentrations; (c, f) ThT fluorescence of given protein in the absence of insulin. *Please note that same insulin*

*aggregation profile is used in all panels of the given condition as the data is derived from the same experiment.*

**Figure S7. BSA does not prevent insulin fibrillation completely, related to Figure 4.** (a) Insulin fibrillation TEM images in the presence of BSA (+/- $Ca^{2+}$).

**Figure S8. SCGN or truncated proteins do not form fibrils, related to Figure 4.** Individual proteins incubated under the amyloidogenic conditions do not form visible fibrils suggesting that the fibrils (seen in TEM images or ThT fluorescence) are the consequence of insulin misfolding and SCGN does not contribute to fibrillation.

**Figure S9. SCGN accelerates insulin internalization, related to Figure 6.** (a) HepG2 (b) N2A cells were incubated with insulin in the presence/absence of SCGN for 1 hour and then free insulin concentration was measured by ELISA; (c) Quantitation of Oil Red O staining of liver sections from HFD treated/untreated animals and control chow group.

**Figure S10. SCGN administration to normal chow-fed animals is largely inconsequential, related to Figure 6.** (a) OGTT; (b) weight gain (c) ITT in SCGN treated/untreated normal chow-fed animals. A trivial change in these parameters upon SCGN administration is noted. In contrast, (d) HFD-fed animals treated with SCGN for the same duration exhibit considerably better insulin tolerance as compared to HFD untreated group.

**Figure S11. SCGN administration to STZ animals does not induce transcriptional changes in the liver, related to Figure 8.** Insulin receptor was significantly upregulated in the liver samples of treated animals. However, the expression of other tested hepatic genes was unperturbed.

**Figure S12. Generation of differentiated, multinuclear C2C12 myotubes, related to transparent methods and Figure 3.** Insulin treatment followed by serum starvation for 48 hours leads to visually appreciable myotube morphology, which is validated by DAPI assisted staining of the nucleus to confirm multinuclear state of myotubes.

Table S1

| Gene Name | Forward Primer (5’-3’) | Reverse Primer (5’-3’) |
|---|---|---|
| IR | CTCTCTGGCAGGAAATGGCT | TTGGCAATATTTGATGGGACATCT |
| FASN | GAGACGCTTCTGGGCTACAG | GGGCAATGCTTGGTCCTTTG |
| GLUCOK | TTGCAACACTCAGCCAGACA | TGAGGATAAGCAGGGGTCGT |
| G6Pase | GGATTCCGGTGTTTGAACGTC | GCAAGGTAGATCCGGGACAG |
| GLUT4 | GCTCTGACGATGGGGAACC | AAACTGAAGGGAGCCAAGCA |
| PEPCK | CCCCCTTGTCTATGAAGCCC | GATCTTGCCCTTGTGTTCTGC |
| SREBP1 | CGGCTCTGGAACAGACACTG | TGAGCTGGAGCATGTCTTCG |
| p85aPI3K | CCTGGACTTAGAGTGTGCCA | GGGCAGTGCTGGTGGAT |
| INS1 | CTGGTGGGCATCCAGTAACC | GTTGAAACAATGACCTGCTTGC |
| INS2 | CCATCAGCAAGCAGGAAGGTTA | GGACTCCCAGAGGAAGAGCA |
| PC1 | CAAGGCCTGTCACCTTGGTA | GCGCTTGTTATTCGCTGGTC |
| SCGN | CGATGTTAGTAAAACTGGAGCCC | CAGATCCACACCACTGATGCT |
| PC2 | TTTGGAGTCCGAAAGCTCCC | GGTGTAGGCTGCGTCTTCTT |
| GLUT2 | GAGATCGCTCCAACCACACT | TGAGGCCAGCAATCTGACTA |
| HPRT1 | CTTCCTCCTCAGACCGCTTT | TCATCGCTAATCACGACGCT |
| ACTB | GCAAGCAGGAGTACGATGAGT | AGGGTGTAAAACGCAGCTCAG |

**Table S1. List of qRT-PCR primers used in this study, related to Figure 8.** Whenever possible, the primers were designed to span exon-exon junction.

**Transparent Methods**

**Antibodies:** Anti-SCGN (bs11754R; Bioss), anti-insulin (bs0855R; Bioss), anti-phospho-Akt (Ser473) rabbit mAb (#9018S; Cell Signalling Technology), anti-Akt (pan) rabbit mAb (#4691S; Cell Signalling Technology), anti-β-actin (bs0061R; Bioss), secondary HRP (bs0295G; Bioss), Alexa Fluor 594 Goat anti rabbit IgG (A11037; Life technologies Molecular probes).

**Pull down assay:** His-tagged SCGN (100 μg) was allowed to bind to a Ni-NTA resin column in the presence of $Ca^{2+}$. MIN6 cells were scrapped in RIPA buffer and sonicated for 10 cycles of 10 sec on/off cycle on a Sonics VibraCell sonicator at 20% efficiency. The whole MIN6 cell lysate was loaded on a SCGN-bound Ni-NTA resin column, washed with PBST buffer and eluted with 250 mM imidazole. The supernatant, wash, and eluents were resolved on 12% SDS-PAGE and gel pieces containing protein bands were excised. The samples were processed for mass spectrometry identification by desalting with zip-tip and analyzed on a Q-Exactive Thermo Scientific mass spectrometer. A protein-free resin control was run similarly. Proteins identified in resin control were considered as background and were excluded from pull down data analysis. Protein identification was performed using Xcalibur software with mouse reference protein databank (UniProt) using a high stringency. Peptide confidence was kept high with precursor mass tolerance of 5 ppm, while fragment mass tolerance was 0.05 Da. Met oxidation was selected as dynamic modification site while Cys carbamidomethylation was set as static modification.

**Cell Culture:** MIN6 cells were cultured in DMEM supplemented with 10% FBS, penicillin (60 mg/lit), and streptomycin (100 mg/lit). HepG2 cells were cultured in similar conditions. C2C12 myocytes were maintained in 20% serum and antibiotics. To differentiate, C2C12 cells were grown in a serum-free DMEM media containing 100 nM insulin. After 24 hours, cells were grown in serum/insulin-free DMEM for 48 hours. The differentiation was assessed by tubular morphology and multinuclear structure by DAPI staining (Fig. S13).

**Colocalization:** MIN6 cells ($0.2x10^6$) were seeded on coverslips in a 6-well plate. After 24 hours, cells were fixed in 4% formaldehyde and immunostained for SCGN and insulin.

Briefly, cells were washed with PBS and permeabilized with 0.1% triton X-100 followed by blocking with 2% BSA at room temperature for 1 hour. Next, the cells were incubated with the anti-insulin antibody (raised in mouse) and anti-SCGN antibody (raised in rabbit) for one hour. After washing thrice with PBST (0.1% Tween 20), cells were incubated with secondary antibodies (goat anti-rabbit Alexa Fluor 594 and goat anti-mouse Alexa Fluor 488) for 1 hour followed by five washes with PBST. DAPI (component of mounting media) was used as a nuclear staining dye. Images were captured on Leica SP8 confocal microscope. Middle three z-sections were stacked with minimum background and contrast correction using Image J software without manipulating any specific feature or part of the image.

**Co-immunoprecipitation (CoIP)**: MIN6 cells were grown in a T75 tissue culture flask and trypsinized upon confluency. The cells collected after slow centrifugation were resuspended in lysis buffer (PBS, 0.1% Tween 20, protCEASE 50; G-Biosciences), and ruptured by three freeze-thaw cycles. and the supernatant was used for immunoprecipitation. For IP from media, 10 ml of conditioned media (from a T75 flask in which 80-90% confluent MIN6 cells were cultured for 24 hours) was concentrated using Amicon Ultrafiltration device (cut-off of 3 kDa). Subsequently, five micrograms of anti-insulin antibody (or 5 µg of irrelevant IgG) was mixed to 1 ml cell lysate (or to media) and incubated overnight at 4 ºC with continuous rotation. Antibody complex was precipitated using Protein A-Sepharose beads (Amersham Biosciences) followed by five washes with PBST. For immunoprecipitation of SCGN-insulin complex from animal plasma, we first incubated anti-insulin antibody with a pre-equilibrated (in PBST) Dynabeads for 2 hours at 4 ºC. After three washes, Dynabead was incubated overnight with mice plasma followed by five washes with PBST. The resin was boiled for 2 minutes in SDS-PAGE loading buffer centrifuged and the supernatant was resolved on 12% SDS-PAGE. The proteins were transferred to a PVDF membrane and developed with the anti-SCGN antibody (1:10,000).

**Recombinant protein purification**: Recombinant SCGN was purified from the soluble fraction on a Ni-NTA column followed by gel filtration by modifying the earlier protocol (Sharma et al., 2019b; Khandelwal et al., 2017; Sharma et al., 2015). Briefly, *E. coli* cells

carrying SCGN expressing vector were grown in minimal media. After 10 hours of post induction (0.5 mM IPTG) incubation at 25 $^{o}$C, the cell pellet was lysed in Buffer A (50 mM Tris, pH 7.5 and 100 mM KCl). After sonication and centrifugal clearance, the supernatant was loaded onto a Ni-NTA column. Bound protein was washed with 8 column volumes of wash buffer 1 (50 mM Tris, pH 7.5, 100 mM KCl) then with the 10-column volumes of wash buffer 2 (50 mM Tris pH 7.5, 100 mM KCl, 2% Triton X100) followed by a wash with wash buffer 1. Protein was eluted with a gradient flow of elution buffer (50 mM Tris, 100 mM KCl, 50-250 mM imidazole gradient). Pure fractions were subjected to size-exclusion chromatography.

For preparing the $Ca^{2+}$ free protein, the gel filtered protein solution was incubated with a 10x molar concentration of EDTA for half an hour followed by exhaustive buffer exchange with Chelex-purified buffer (50 mM Tris, pH 7.5, 100 mM KCl). For animals and cell culture experiments, the protein was buffer exchanged to PBS, filtered with 0.22 µ syringe filter and aliquots were stored in -80 $^{o}$C at 2 mg/ml concentration.

ΔNTD SCGN (amino acid 104-276) and ΔCTD SCGN (amino acid 1-186) were constructed by cloning respective amino acids with appropriate primers into pET21b vector. ΔCTD was purified by anion exchange (Q-Sepharose; Tris, pH 8.5) chromatography while ΔNTD was purified by hydrophobic interaction chromatography (Phenyl-Sepharose; Tris pH 7.5) followed by anion exchange chromatography (Q-Sepharose; Tris, pH 7.5). The details of the truncated protein purification protocol are available on request. All proteins were then subjected to size exclusion chromatography on a Sephadex G-75 (GE Healthcare) column in 50 mM Tris, pH 7.5, 100 mM KCl buffer. Decalcification was essentially same as for the full-length SCGN.

**Protein overlay assay:** The proteins were immobilized on a PVDF membrane with a slot-blot manifold apparatus (Amersham Biosciences). After blocking with 5% BSA, the membrane was incubated with 10 µM SCGN for one hour and washed four times with PBST. The further procedure was followed as standard Western Blotting with the anti-SCGN antibody (1:10,000 dilution).

To assess insulin binding to truncated SCGN, 10 µM protein samples were immobilized on PVDF membrane. After blocking with 5% BSA, membrane was

incubated with 100 µM insulin. Downstream processing was done as described above except that the anti-insulin antibody was used to probe insulin binding to truncated proteins.

**Bio-layer interferometry:** BLI experiments were performed on an Octet Red 96 system. Our efforts to immobilize His-tagged-SCGN using Ni-NTA chemistry or using amine-coupling chemistry were unsuccessful because of non-specific binding of insulin to either probe. We hence immobilized insulin (100 µg) on the probe using amine-coupling and 200 µl SCGN (100 µM) was taken as a ligand in the wells in the $Ca^{2+}$ free (100 µM EDTA) or $Ca^{2+}$ saturated (1 mM $Ca^{2+}$) form. Initial baseline-60 s, association/dissociation- 300 s each followed by a regeneration step. Two controls were run (i) insulin-immobilized probe and buffer in the well, (ii) free inert probe with SCGN in the well. There was an inappreciable signal in the control (i). Reference (ii) was subtracted from the sample. The data fitting was performed for the initial 120 seconds of association phase and 300 seconds of dissociation phase in the vendor-supplied module using 1:1 model. The $R^2$ of >0.95 and $Chi^2$ of <1 was used as the criteria of a good fit.

**Spectral measurements:** Circular dichroism (CD) spectra were recorded on a Jasco J-815 spectropolarimeter using 1 cm path length cuvettes. Fluorescence emission spectra were recorded on an F-7000 Hitachi spectrophotometer at an excitation wavelength of 295 nm. The excitation and emission band passes were set at 5 nm and spectra were recorded in 50 mM Tris (pH 7.5), 100 mM KCl. The spectra were corrected for insulin contribution. Near-UV CD spectra were recorded using 1 mg/ml protein concentration, and fluorescence spectra were recorded using 0.1 mg/ml protein (unless otherwise stated in the graph).

**Analytical gel filtration:** Differential elution of proteins and their complex were resolved on a Superdex 75 (10/300) column (Wipro GE Healthcare) under described conditions. Column was pre-equilibrated with buffer (50 mM Tris, pH 7.5, 100 mM KCl) containing either 0.1 mM EDTA or 2 mM $Ca^{2+}$.

**Insulin amyloidogenesis by TEM**: Either the proteins or their complex were incubated overnight at 60 ºC without stirring. Fibrils thus formed were mixed using a 200 microliter pipette. The solution was applied onto a 300-mesh copper grid and stained with freshly prepared uranyl acetate (2%). Dried samples were observed under a transmission electron microscope (Hitachi, Japan) operating at an accelerating voltage of 200 kV.

**Insulin amyloidogenesis and aggregation by fluorescence spectroscopy**: For the real-time insulin fibrillation measurement, 85 µM insulin or insulin + SCGN combination (50 mM glycine, 100 mM KCl, pH 2.5, 10 µM ThT) was incubated at 55 ºC (in the absence of $Ca^{2+}$) or 60 ºC (in the presence of $Ca^{2+}$) with continuous stirring. ThT fluorescence was monitored for one hour ($\lambda_{ex}$ =440 nm, $\lambda_{em}$=482 nm). For DTT-induced aggregation, 40 µM insulin (in 50 mM Tris buffer, pH 7.5, 100 mM KCl) in the presence or the absence of different concentrations of SCGN was equilibrated at 37 °C for 10 min with constant stirring in the cuvette.. The reduction of insulin was initiated by the addition of 20 mM DTT to the sample. The extent of aggregation was monitored as scattering (excitation and emission monochromators set at 465 nm) set at 5 nm band passes in time scan mode of the instrument.

For a large set of proteins (BSA, full length and truncated SCGN in the presence/absence of SCGN), we measured the extent of insulin fibrillation at regular time intervals while the samples were on a temperature controlled orbital shaker at 300 rpm at 55 ºC (in the presence of 250 µM EDTA) or 60 ºC (in the presence of 1 mM $Ca^{2+}$). Protein samples were prepared in amyloidogenesis buffer (50 mM glycine pH 2.5, 100 mM KCl, 50 µM ThT) in a 96-well plate. BSA was taken as control (Finn et al., 2012). ThT fluorescence was measured periodically on a Perkin-Elmer multimode Plate reader in triplicate and standard error was calculated from triplicate values.

**MTT assay:** Fibrils were generated by overnight incubation of 1 mg/ml insulin in 50 mM glycine pH 2.5, 100 mM KCl buffer at 65 ºC. MIN6 cells were seeded at a density of 20,000 cells/well in a 96-well plate. Next day, the cells were washed with PBS and incubated with 10 µM SCGN, 20 µM insulin fibrils (fibrils), a complex of 10 µM SCGN and 20 µM fibrils, 5% Triton X-100 (negative control), or BSA and fibrils complex in serum-free media for 24 hours. Cells were washed again with PBS and incubated with 100

µl of 5 mg/ml MTT in incomplete media for 4 hours at 37 ºC. Fifty microliters of media were replaced with DMSO and mixed properly to dissolve crystals. The absorbance was recorded at 540 nm on a Perkin-Elmer multimode Plate reader. The number of samples per treatment was eight (n=8).

**Modelling SCGN-insulin complex**- A 3-D model of mouse SCGN was generated by Phyre2 (Protein Homology/analogY Recognition Engine V 2.0) (Kelley et al., 2015) using zebrafish SCGN structure (PDB id: 2Q4U) as a template. mSCGN model was used as a receptor molecule and insulin (PDB 5EN9) was the ligand for generating a docking model by Patchdoc server (Schneidman-Duhovny et al., 2005) while accepting the default settings. The resultant model was analyzed on the Pymol software.

**FITC-Insulin preparation:** Five-milligram insulin powder was dissolved in 1 ml glycine buffer (50 mM glycine, 100 mM KCl, pH 2.5, 1 mM EDTA) to avoid insulin aggregation. After insulin was dissolved, the solution was diluted 4 times. In parallel, 2 mg FITC was dissolved in 300 µl ethanol. FITC was added drop wise to the insulin solution on a magnetic stirrer in dark at room temperature. After 3 hours of the coupling reaction, the solution was subjected to a size exclusion column attached to a Bio-Rad FPLC system. Pure insulin fractions were decided by the absorbance at 280 and 495 nm set in a Quadtec detector. The extent of FITC conjugation was calculated exactly as recommended by the SIGMA (CAS #: 3326-32-7). Our preparation was found to have ~4 FITC molecules per insulin molecule.

**FACS assisted quantification of 2-NBDG**: HepG2 cells were cultured in six-well plates. After cells reach ~80% confluency, cells were kept in glucose-free KRP buffer for overnight fasting/glucose deprivation. Subsequently, cells were subjected to the following treatment: 40 µM 2-NBDG, 100 nM insulin, 100 nM SCGN, a complex of SCGN and insulin in glucose-free KRP buffer for 2 hours. Control samples did not receive any treatment except the corresponding buffer. The cells were washed with PBS and processed for FACS analysis essentially as described in the previous section.

**Microscopic and FACS study of FITC-insulin internalization:** HepG2 cells were seeded on the coverslips in a six-well plate **(**$0.2x10^6$ cells/well). After cells reached ~80-90% confluency, the cells were serum deprived for 24 hours and were treated with 10 µM FITC-insulin either in the presence or absence of 10 µM of unlabelled SCGN. After 30 min incubation, the culture plate was transferred to the ice and was washed thrice with ice-cold PBS followed by two washes with ice-cold glycine-NaCl buffer (120 mM glycine, 150 mM NaCl, pH 2.5) to remove membrane-bound FITC-insulin. After additional two washes with ice-cold PBS, cells on coverslips were fixed and mounted on a glass slide with DAPI containing mounting media. For better visualization, DAPI was pseudo-colored to red instead of conventional blue color. The images were captured on an Apotome 2 system with 63x objective and oil immersion medium. The exposure time for each channel was constant for all the samples. No image processing was performed on the acquired images.

For FACS-assisted quantification of FITC-insulin internalization, samples were prepared similarly except that coverslips were not used for FACS samples. After the washes, the cells were trypsinized, centrifuged and the cell pellet was resuspended in 400 µl PBS. Immediately, FACS analysis was performed on a Beckman Coulter Gallios Flow Cytometer system using FITC channel. At least 20,000 cells were analyzed for each sample. The data analysis and figure preparation were performed by Kaluza software module provided by the vendor.

**ELISA for insulin internalization:** HepG2 or N2A cells (0.2 million cells/well) were seeded in a six well plate. After 24 hours, serum free mediated containing 100 ng/ml insulin alone or with 1 µg/ml SCGN was added to three wells. After one hour of incubation, mediated samples were taken and were used for ELISA quantification of free insulin in media.

**Akt phosphorylation assay:** C2C12 cells were differentiated in T25 cell culture flasks. Differentiation was induced by incubating C2C12 myoblast in serum free media supplemented with 100 nM insulin. After 24 hours, the cells were incubated in serum free media for another 48 hours which leads to differentiated C2C12 myotube formation (Fig. S12). After glucose deprivation (2 hours for C2C12 and 4 hours for HepG2 cells) in

glucose-free KRP (20 mM HEPES, 0.4 mM $K_2HPO_4$, 1 mM $MgSO_4$, 5 mM KCl, 135 mM NaCl), the cells were washed thrice and treated with insulin (100 nM) or SCGN (100 nM) or with a complex of the two in KRP buffer. Control samples received the corresponding buffer. After 20 minutes, cells were lysed in RIPA buffer. Total protein was quantified by BCA method and 50 µg protein was resolved on two parallel 12% SDS-PAGE gels followed by Western blotting. One blot was processed for pAkt (Ser473) antibody (1:10,000) while other blot was used for co-detection of β-actin (1:10,000) and Akt (1:10,000) with respective antibodies. Densitometry analysis was performed with Image J software. The pAkt/Akt values were first normalized with corresponding actin values and then a ratio of normalized pAkt/Akt was calculated using Microsoft excel software.

**Animal maintenance, OGTT and ITT:** Animals (after due approval from the Institutional Animal Ethics Committee, approval numbers 91/2015, 2/2017 and 35/2017) were maintained in *Individually Ventilated Cages. BALB/c* mice were kept *on normal chow, C57BL/6J mice were fed either normal chow (control group) or HFD. To induce diabetes in BALB/c* mice, STZ (100 mg/kg bodyweight in citrate buffer pH 4.5) was injected intraperitoneally after six hours of fasting. After 3 days, glucose level was measured and animals showing random glucose >200 mg/dL were selected for experiments. *C57BL/6J* mice were maintained on a high-fat diet (HFD; D12492, Research Diets, New Brunswick, NJ) or normal chow and the SCGN treatment was started simultaneously. After three months, the first set of OGTT and ITT experiments were performed.

OGTT was conducted after overnight fasting. Mice were fed an oral bolus of 2 g glucose per kilogram body weight and blood glucose was monitored at every 30 min using an AccuCheck active OneTouch glucometer (Roche).

ITT was conducted after 6 h of fasting. Mice were injected with (i.p.) 0.75 IU of fast acting insulin per kilogram body weight and blood glucose was monitored at every 20 min using an AccuCheck active OneTouch glucometer (Roche).

**Serum Analysis:** Random triglyceride (GPO/PAP method, TG kit, Coral Clinical Systems), cholesterol (CHOD/PAP method, CHOL Kit, Coral Clinical Systems), HDL (Direct enzymatic method, HDL-D kit, Coral Clinical Systems), $Ca^{2+}$ (OCPC method,

CAL Kit, Coral Clinical Systems) and glucose (Glucose (GO) assay kit; cat: GAGO20-1KT, SIGMA) were measured as per the product guidelines and protocols. LDL level was calculated by the equation: (Total Cholesterol) – (HDL) – (TG/5).

**ELISA:** Insulin (Ultra-Sensitive Mouse Insulin ELISA kit, Crystal Chem; cat: 90080) and SCGN (Secretagogin BioAssay™, USBiological; cat: 027968) measurements were performed as per the vendor's guidelines following the product protocols.

**Insulin sensitivity index [$ISI_{(0,\ 120)}$]:** The insulin sensitivity index was calculated precisely as described (28). Briefly, after 16 hours of fasting, blood was drawn for serum insulin/glucose measurements. Two hours after the oral glucose bolus (as described in OGTT), another sample of blood was collected. Serum glucose and insulin levels were determined as described in respective sections. Metabolic Clearance Rate (MCR) and Mean Serum Insulin (MSI) were calculated and insulin sensitivity was calculated as $ISI_{0,120}$= MCR/log MSI.

**Oil Red O staining:** Frozen liver tissues were sectioned on a microtome at the thickness of 5 micrometers and immobilized on charged slides. Oil Red O (SIGMA, O1391-250ML) staining was performed as follows. Tissues were soaked in distilled water followed by a wash with PBS. Then slides were dipped in 60% isopropanol followed by immersion in Oil Red O solution for 1 hour. Next, slides were washed twice with PBS (5 min each) followed by immersion in hematoxylin solution for 4 minutes. Finally, slides were washed in running tap water and glycerol soaked tissues were covered with coverslips. Slides were observed under an Axioplan 2 imaging system. Quantitation of oil red stained pixels was performed using ImageJ software. Three animals were arbitrarily selected from each group. For every sample, $ORO^{+}$ pixels from seven fields were average. Students t-test was performed on averaged values (*i.e.* n=3).

**Echo-MRI:** EchoMRI™-500, which is designed to analyze the body composition for live small animals, was used for total fat content measurements. Animals were maintained in vendor provided animals restrainer. All readings were the average of three accumulations.

**Histology:** At the end of experiments (and after a recovery period), animals were sacrificed using recommended procedures. Tissues were excised and fixed in formalin (10% formaldehyde in phosphate-buffered) followed by processing and embedding. The paraffin-embedded tissues were sectioned at 4-micrometer thickness. Sections were stained with hematoxylin and eosin and were visualized on an Axioplan 2 imaging system.

**qRT-PCR:** Tissue samples, immediately after removal from animals, were washed and immersed in TRIzol RNAiso plus reagent and stored at -80 ºC. At the time of processing, tissues were thawed and total RNA was isolated by chloroform extraction. Upon checking the integrity and concentration of RNA, 5 µg of RNA was used for cDNA synthesis using SuperScript III First-Strand Synthesis System (Thermo Fisher Scientific). mRNA levels were quantified by qRT-PCR (ABI Prism 7900 HT; Applied Biosystems) using SYBR Green (Applied Biosystems). The primer sequence for analyzed genes is appended in the supplementary information (Table. S1).

**Statistical analysis:** All significance tests for group-wise comparison were performed on MS excel using student's t-test except OGTT and ITT time course measurements where two-way ANOVA analyses (with Holm-Sidak post-hoc analysis) were performed on the Sigma plot software.

**Supplementary references**

Kelley LA, Mezulis S, Yates CM, Wass MN, Sternberg MJE (2015) The Phyre2 web portal for protein modeling, prediction and analysis. *Nature Protocols,* 10, 845-858.